Semi-Discrete Central-Upwind Schemes for Hyperbolic Conservation Laws and Hamilton-Jacobi Equations

Alexander Kurganov[†], Sebastian Noelle[‡] and Guergana Petrova[†]

Abstract

We introduce new Godunov-type semi-discrete central schemes for hyperbolic systems of conservation laws and Hamilton-Jacobi equations. The schemes are based on the use of more precise information about the local speeds of propagation, and can be viewed as a generalization of the schemes from [26, 24, 25] and [27].

The main advantages of the proposed central schemes are the high resolution, due to the smaller amount of the numerical dissipation, and the simplicity. There are no Riemann solvers and characteristic decomposition involved, and this makes them a universal tool for a wide variety of applications.

At the same time, the developed schemes have an upwind nature, since they respect the directions of wave propagation by measuring the *one-sided* local speeds. This is the reason why we call them *central-upwind* schemes.

The constructed schemes are applied to various problems, such as the Euler equations of gas dynamics, the Hamilton-Jacobi equations with convex and nonconvex Hamiltonians, and the incompressible Euler and Navier-Stokes equations. The incompressibility condition in the latter equations allows us to treat them both in their conservative and transport form. We apply to these problems the central-upwind schemes, developed separately for each of them, and compute the corresponding numerical solutions. The obtained results demonstrate the advantage of our new central-upwind approach.

AMS subject classification: Primary 65M06; Secondary 35L65

Key Words: Multidimensional conservation laws and Hamilton-Jacobi equations, high-resolution semi-discrete central schemes, compressible and incompressible Euler equations.

Contents

[†]Department of Mathematics, University of Michigan, Ann Arbor, MI 48109-1109, USA. Email addresses: kurganov@math.lsa.umich.edu, petrova@math.lsa.umich.edu
[‡]Institute of Applied Mathematics, Bonn University, 53115 Bonn, Germany. Email address: noelle@iam.uni-bonn.de

1 Introduction

We consider Godunov-type schemes for the multidimensional systems of conservation laws

$$u_t + \nabla_{\mathbf{x}} \cdot f(u) = 0, \quad \mathbf{x} \in I\!R^d, \tag{1.1}$$

and the multidimensional Hamilton-Jacobi equations

$$\varphi_t + H(\nabla_{\mathbf{x}}\varphi) = 0, \quad \mathbf{x} \in I\!R^d. \tag{1.2}$$

Godunov-type schemes for the system (1.1) are projection-evolution methods. Starting with cell averages at time level t^n, one reconstructs a piecewise polynomial interpolant of degree $r-1$ (where r is the formal order of the scheme), which is evolved to the next time level t^{n+1}, and then it is projected onto a space of piecewise constants. Depending on the projection step, we distinguish two kinds of Godunov-type schemes – central and upwind. The Godunov-type central schemes are based on exact evolution and averaging over Riemann fans. In contrast to the upwind schemes, they do not employ Riemann solvers and characteristic decomposition, which makes them *simple, efficient* and *universal.*

In the one-dimensional case, examples of such schemes are the first-order (staggered) Lax-Friedrichs scheme [28, 14], the second-order Nessyahu-Tadmor scheme [40], and the higher-order schemes in [39, 8, 30]. Second-order multidimensional central schemes were introduced in [3, 4, 5, 6, 19, 34], and their higher-order extensions were developed in [31, 32]. We would also like to mention the central schemes for incompressible flows in [33, 22, 20, 21], and their applications to various systems, for example, [2, 13, 44, 49].

Unfortunately, these staggered central schemes may not provide a satisfactory resolution when small time steps are enforced by stability restrictions, which may occur, for example, in the application of these schemes to convection-diffusion problems. Also, they cannot be used for steady-state computations. These disadvantages are caused by the accumulation of numerical dissipation, which is of order $\mathcal{O}(\frac{(\Delta x)^{2r}}{\Delta t})$, where r is the formal order of the scheme.

The aforementioned problems have been recently resolved in [26], where new high-order Godunov-type central schemes are introduced. The proposed construction is based on the use of the CFL related *local speeds of propagation* and on integration over Riemann fans of variable sizes. In this way, a *non-staggered* fully-discrete central scheme is derived and it is naturally reduced to a particularly simple semi-discrete form (for details see [26]). The same idea was used in [24] to develop a third-order semi-discrete central scheme, and in [25], where its genuinely multidimensional extension was introduced.

The purpose of the first part of this paper is to present new semi-discrete central schemes for the conservation law (1.1), which we call *central – upwind* schemes. They are based on the *one-sided local speeds of propagation.* For example, in the one-dimensional case, these one-sided local speeds are the largest and smallest eigenvalues of the Jacobian $\frac{\partial f}{\partial u}$ (in contrast to the less precise local information, used in [26, 24, 25] – the spectral radius $\rho(\frac{\partial f}{\partial u})$).

The new schemes are Godunov-type *central* schemes, because the evolution step employs integration over Riemann fans and does not require a Riemann solver and a characteristic decomposition. They also have an *upwind* nature, since a one-sided information is used to estimate the width of the Riemann fans. This more precise estimate makes our schemes less dissipative generalizations of the semi-discrete central schemes in [26, 24, 25].

The second part of this paper is devoted to the Hamilton-Jacobi equations (1.2). Examples of numerical methods for these equations can be found in [1, 10, 11, 35, 36, 42, 48]. One of the approaches ([35, 36]) is Godunov-type schemes. As in the case of conservation laws, they are projection-evolution methods. The differences are that here one starts with point values (not cell averages) at time t^n, builds a *continuous* piecewise polynomial reconstruction of degree r, and evolves it to the next time level t^{n+1}. The pointwise projection (not the cell averages) of this evolved solution is used as initial data for the next time step.

Godunov-type central schemes for Hamilton-Jacobi equations were first introduced in [35, 36]. Semi-discrete Godunov-type central schemes for the multidimensional equations (1.2) were developed in [27], where the same idea of *local speeds of propagation* was used to separate between smooth and nonsmooth parts of the evolved solution.

In the second part of this work, we present a new second-order semi-discrete *central-upwind* scheme for the Hamilton-Jacobi equations (1.2). It is a less dissipative generalization of the scheme in [27], which uses a more precise one-sided information of the local propagation speeds.

The paper is organized as follows. In Section 2, we give a brief overview of the Godunov-type central schemes for conservation laws and Hamilton-Jacobi equations in one space dimension. We also describe the non-oscillatory piecewise quadratic reconstruction from [25], which is later used in the numerical examples. Next, in Section 3, we introduce our new Godunov-type *central – upwind* schemes for the conservation laws and Hamilton-Jacobi equations, both in one and in two spatial dimensions. The results of our numerical experiments are presented in Section 4. We apply the proposed scheme to a variety of test problems: the one- and two-dimensional compressible Euler equations, a one-dimensional Hamilton-Jacobi equation with a nonconvex Hamiltonian, the two-dimensional eikonal equation of geometric optics. Finally, the incompressible Euler and Navier-Stokes equations are solved using two different approaches, based on either their conservative or transport form. The performed numerical experiments, especially in the case of incompressible flow simulations (see Section 4.4), demonstrate the advantage of our new central-upwind approach.

2 Godunov-type central schemes – brief description

In this section, we review Godunov-type central schemes in one spatial dimension. In Section 2.1, we recall the construction of staggered central schemes for conservation laws. High-order Godunov-type schemes employ high-order piecewise polynomial reconstructions. In Section 2.2, we recall an example of a one-dimensional non-oscillatory piecewise parabolic reconstruction, proposed in [25]. Finally, in Section 2.3, we review the Godunov-type central schemes for Hamilton-Jacobi equations. In Section 3, we will introduce our new semi-discrete central-upwind schemes, both in one and in two space dimensions.

We will consider only uniform grids and use the following notation – let $x_j := j\Delta x$, $x_{j\pm\frac{1}{2}} := (j \pm 1/2)\Delta x$, $t^n := n\Delta t$, $u_j^n := u(x_j, t^n)$, $\varphi_j^n := \varphi(x_j, t^n)$, where Δx and Δt are small spatial and time scales, respectively.

2.1 Central schemes for conservation laws

The starting point for the construction of Godunov-type schemes for conservation laws is the equivalent integral formulation of the system (1.1),

$$\bar{u}(x,t+\Delta t)=\bar{u}(x,t)-\frac{1}{\Delta x}\left[\int\limits_{\tau=t}^{t+\Delta t} f(u(x+\frac{\Delta x}{2},\tau))\,d\tau-\int\limits_{\tau=t}^{t+\Delta t} f(u(x-\frac{\Delta x}{2},\tau))\,d\tau\right], \tag{2.1}$$

where by

$$\bar{u}(x,t):=\frac{1}{\Delta x}\int\limits_{I(x)} u(\xi,t)\,d\xi, \qquad I(x)=\{\xi:|\xi-x|<\frac{\Delta x}{2}\} \tag{2.2}$$

we denote the sliding averages of $u(\cdot,t)$ over the interval $(x-\frac{\Delta x}{2},x+\frac{\Delta x}{2})$. At time level $t=t^n$ we consider problem (2.1) with the piecewise polynomial initial condition

$$\widetilde{u}(x,t^n)=p_j^n(x), \qquad x_{j-\frac{1}{2}}<x<x_{j+\frac{1}{2}}, \quad \forall j, \tag{2.3}$$

obtained from the cell averages $\bar{u}_j^n:=\bar{u}(x_j,t^n)$, computed at the previous time step. This piecewise polynomial reconstruction should be conservative, accurate of order r, and non-oscillatory. Different reconstructions are discussed in Section 2.2.

Then, the piecewise polynomial $\widetilde{u}(x,t^n)$ is evolved exactly according to (2.1), and the solution at time $t=t^{n+1}$ is obtained in terms of its sliding averages, $\bar{u}(x,t^{n+1})$. An evaluation of these sliding averages at particular grid points provides the approximate cell averages of the solution at the next time level.

The choice of $x=x_j$ in (2.1) results in an upwind scheme. The solution then may be non-smooth in the neighborhood of the points $\{x_{j+\frac{1}{2}}\}$ and the evaluation of the flux integrals in (2.1) requires the use of a computationally expensive (approximate) Riemann solver and characteristic decomposition.

If $x=x_{j+\frac{1}{2}}$ in (2.1), we obtain Godunov-type central schemes, namely

$$\begin{aligned}\bar{u}_{j+\frac{1}{2}}^{n+1} &= \frac{1}{\Delta x}\left[\int\limits_{x_j}^{x_{j+\frac{1}{2}}} p_j^n(x)\,dx+\int\limits_{x_{j+\frac{1}{2}}}^{x_{j+1}} p_{j+1}^n(x)\,dx\right]- \\ &- \frac{\lambda}{\Delta t}\left[\int\limits_{t^n}^{t^{n+1}} f(u(x_{j+1},t))\,dt-\int\limits_{t^n}^{t^{n+1}} f(u(x_j,t))\,dt\right], \quad \lambda:=\frac{\Delta t}{\Delta x}.\end{aligned} \tag{2.4}$$

In contrast to the upwind framework, the solution is smooth in the neighborhood of the points $\{x_j\}$. Therefore, a discretization of the flux integrals in (2.4) can be done, using an appropriate quadrature formula. The corresponding function values can be computed either by Taylor expansion, or by a Runge-Kutta method ([39, 8]).

2.2 Non-oscillatory piecewise polynomial reconstructions

As we have already mentioned, one of the three building blocks of Godunov-type schemes for conservation laws is a piecewise polynomial reconstruction. Second-order schemes require a piecewise linear reconstruction (see the examples in [15, 16, 23, 29, 40, 43]). Third-order schemes employ a piecewise quadratic approximation, and one of the possibilities is to use the essentially non-oscillatory (ENO) reconstruction. In the one-dimensional case we refer the reader to [16, 46]. The weighted ENO interpolants are proposed in [38, 18, 30, 32], and the multidimensional ENO-type reconstructions can be found in [31, 32]. The ENO-type approach employs smoothness indicators. They require a certain a-priori information about the solution, which may be unavailable and then spurious oscillations or extra smearing of discontinuities may appear.

One-dimensional non-oscillatory piecewise quadratic reconstructions, which do not require the use of smoothness indicators, were proposed in [37, 39, 25]. Two-dimensional generalizations of these reconstructions were presented in [25, 41].

For completeness, we give a brief description of the one-dimensional third-order non-oscillatory reconstruction from [25], which we will use later on in our numerical experiments for one-dimensional conservation laws. We denote by $D_\pm$ and D_0 the one-sided and the central divided differences

$$D_\pm v(x) := \pm\frac{v(x\pm\Delta x)-v(x)}{\Delta x}, \qquad D_0 v(x) := \frac{v(x+\Delta x)-v(x-\Delta x)}{2\Delta x},$$

and consider the basic piecewise quadratic reconstruction

$$q_j^n(x) = (\bar u_j^n - \frac{(\Delta x)^2}{24}D_+D_-\bar u_j^n) + D_0\bar u_j^n(x-x_j) + \frac{1}{2}D_+D_-\bar u_j^n(x-x_j)^2, \quad x\in(x_{j-\frac12},x_{j+\frac12}), \tag{2.5}$$

which is *conservative*, *accurate*, and satisfies a *shape-preserving* property (for details, see [39, 25]). Unfortunately, this reconstruction is, in general, oscillatory since new extrema may be created at the interface points $\{x_{j+\frac12}\}$. To prevent this, a convex combination of the basic parabolas q_j^n and the piecewise linear interpolant L_j^n is used, namely

$$p_j^n(x) = (1-\theta_j^n)L_j^n(x) + \theta_j^n q_j^n(x), \qquad 0<\theta_j^n<1, \tag{2.6}$$

where

$$L_j^n(x) = \bar u_j^n + s_j^n(x-x_j). \tag{2.7}$$

An appropriate choice of $\{\theta_j^n\}$ and $\{s_j^n\}$ guarantees the non-oscillatory property of the new piecewise quadratic reconstruction $\{p_j^n\}$ (see [25]). We take $\{\theta_j^n\}$ to be

$$\theta_j^n := \begin{cases} \min\left\{\dfrac{M_{j+\frac12}^n - L_j^n(x_{j+\frac12})}{M_j^n - L_j^n(x_{j+\frac12})}, \dfrac{m_{j-\frac12}^n - L_j^n(x_{j-\frac12})}{m_j^n - L_j^n(x_{j-\frac12})}, 1\right\}, & \text{if } \ \bar u_{j-1}^n < \bar u_j^n < \bar u_{j+1}^n, \\ \min\left\{\dfrac{M_{j-\frac12}^n - L_j^n(x_{j-\frac12})}{M_j^n - L_j^n(x_{j-\frac12})}, \dfrac{m_{j+\frac12}^n - L_j^n(x_{j+\frac12})}{m_j^n - L_j^n(x_{j+\frac12})}, 1\right\}, & \text{if } \ \bar u_{j-1}^n > \bar u_j^n > \bar u_{j+1}^n, \\ 1, & \text{otherwise}, \end{cases} \tag{2.8}$$

where

$$M_j^n = \max\left\{q_j^n(x_{j+\frac12}), q_j^n(x_{j-\frac12})\right\}, \qquad m_j^n = \min\left\{q_j^n(x_{j+\frac12}), q_j^n(x_{j-\frac12})\right\},$$

and

$$\begin{aligned} M_{j\pm\frac12}^n &= \max\left\{\frac12\Big(L_j^n(x_{j\pm\frac12}) + L_{j\pm1}^n(x_{j\pm\frac12})\Big), q_{j\pm1}^n(x_{j\pm\frac12})\right\}, \\ m_{j\pm\frac12}^n &= \min\left\{\frac12\Big(L_j^n(x_{j\pm\frac12}) + L_{j\pm1}^n(x_{j\pm\frac12})\Big), q_{j\pm1}^n(x_{j\pm\frac12})\right\}. \end{aligned}$$

Our choice of the non-oscillatory piecewise linear approximation $\{L_j^n\}$ is the standard *minmod* interpolant (2.7) (see [29, 15, 43]) with

$$s_j^n = \text{minmod}\left(\frac{\bar u_j^n - \bar u_{j-1}^n}{\Delta x}, \frac{\bar u_{j+1}^n - \bar u_j^n}{\Delta x}\right), \tag{2.9}$$

where

$$\operatorname{minmod}(a,b) := \frac{\operatorname{sgn}(a)+\operatorname{sgn}(b)}{2}\min(|a|,|b|).$$

If one sets all slopes s_j^n to be zero, then (2.6)–(2.8) is reduced to the original reconstruction from [39]. The final piecewise parabolic reconstruction is

$$p_j^n(x) = \Big(\bar{u}_j^n - \theta_j^n\frac{(\Delta x)^2}{24}D_+D_-\bar{u}_j^n\Big) + \Big(\theta_j^n D_0\bar{u}_j^n + (1-\theta_j^n)s_j^n\Big)(x-x_j) + \frac{\theta_j^n}{2}D_+D_-\bar{u}_j^n(x-x_j)^2, \quad (2.10)$$

where θ_j^n and s_j^n are given by (2.8) and (2.9), respectively.

2.3 Central schemes for Hamilton-Jacobi equations

In this section, we describe a second-order Godunov-type central schemes for Hamilton-Jacobi equations. We follow the approach from [36] and construct a one-dimensional second-order staggered central scheme.

Assume that we have computed the point values of φ at time $t = t^n$. We then start with a continuous piecewise quadratic interpolant,

$$\widetilde{\varphi}(x,t^n) := \varphi_j^n + \frac{(\Delta\varphi)^n_{j+\frac12}}{\Delta x}(x-x_j) + \frac{(\Delta\varphi)'_{j+\frac12}}{2(\Delta x)^2}(x-x_j)(x-x_{j+1}), \quad x\in[x_j,x_{j+1}], \quad (2.11)$$

where

$$(\Delta\varphi)^n_{j+\frac12} := \varphi^n_{j+1} - \varphi^n_j. \quad (2.12)$$

Here, $(\Delta\varphi)'_{j+\frac12}/(\Delta x)^2$ is an approximation to the second derivative $\varphi_{xx}(x_{j+\frac12},t^n)$. An appropriate *nonlinear limiter*, employed in this approximation guarantees the non-oscillatory nature of $\widetilde{\varphi}(x,t^n)$. Examples of such limiters, developed in the context of hyperbolic conservation laws, may be found in [15, 16, 23, 40, 43]. In this paper we use a one-parameter family of the *minmod* limiters, [29, 15, 43],

$$(\Delta\varphi)'_{j+\frac12} = \operatorname{minmod}\left(\theta((\Delta\varphi)^n_{j+\frac32}-(\Delta\varphi)^n_{j+\frac12}), \frac12((\Delta\varphi)^n_{j+\frac32}-(\Delta\varphi)^n_{j-\frac12}), \theta((\Delta\varphi)^n_{j+\frac12}-(\Delta\varphi)^n_{j-\frac12})\right), \quad (2.13)$$

where $\theta\in[1,2]$, and the multivariable minmod function is defined by

$$\operatorname{minmod}(x_1,x_2,...) := \begin{cases}\min_j\{x_j\}, & \text{if } x_j>0 \ \ \forall j,\\ \max_j\{x_j\}, & \text{if } x_j<0 \ \ \forall j,\\ 0, & \text{otherwise.}\end{cases} \quad (2.14)$$

Notice that larger θ's in (2.13) correspond to less dissipative, but still *non-oscillatory* limiters, [29, 15, 43].

Given a reconstruction (2.11), we consider the Hamilton-Jacobi equation (1.2), subject to the initial data $\varphi(x,0)=\widetilde{\varphi}(x,t^n)$. Under an appropriate CFL condition, due to the finite speed of propagation, the solution of this initial value problem is smooth in the neighborhood of the line segment $\{(x,t): x = x_{j+\frac12},\ t^n\le t\le t^{n+1}\}$. Therefore, from the Taylor expansion of the solution about the point $(x_{j+\frac12},t^n)$, we obtain

$$\varphi^{n+1}_{j+\frac12} = \frac{\varphi^n_j+\varphi^n_{j+1}}{2} - \frac{(\Delta\varphi)'_{j+\frac12}}{8} - \Delta t H\left(\frac{(\Delta\varphi)^n_{j+\frac12}}{\Delta x}\right) + \frac{(\Delta t)^2}{2}\left[H'\left(\frac{(\Delta\varphi)^n_{j+\frac12}}{\Delta x}\right)\right]^2\cdot\frac{(\Delta\varphi)'_{j+\frac12}}{(\Delta x)^2}. \quad (2.15)$$

Remarks.

1. The derived scheme (2.15) is different from the one in [36]. There, the evolution step is executed by integration of (1.2) over $[t^n, t^{n+1}]$, followed by the application of the mid-point rule to the resulting integrals. For details, see [36, 27].
2. A two-dimensional staggered central scheme for (1.2) can be found in [36].

3 Central-upwind semi-discrete schemes

In this Section we develop new semi-discrete central-upwind schemes for conservation laws and Hamilton-Jacobi equations, following the approach presented in [26, 24, 25] and [27], respectively.

3.1 Semi-discrete central-upwind schemes for one-dimensional conservation laws

We consider the one-dimensional system (1.1) of N strictly hyperbolic conservation laws. We start with a piecewise polynomial reconstruction (2.3) with possible discontinuities at the interface points $\{x_{j+\frac{1}{2}}\}$. These discontinuities propagate with right- and left-sided local speeds, which can be estimated by

$$a^+_{j+\frac{1}{2}} := \max_{\omega\in C(u^-_{j+\frac{1}{2}},u^+_{j+\frac{1}{2}})} \Big\{\lambda_N\Big(\frac{\partial f}{\partial u}(\omega)\Big),0\Big\},$$

and

$$a^-_{j+\frac{1}{2}} := \min_{\omega\in C(u^-_{j+\frac{1}{2}},u^+_{j+\frac{1}{2}})} \Big\{\lambda_1\Big(\frac{\partial f}{\partial u}(\omega)\Big),0\Big\},$$

respectively. Here, $\lambda_1 < \ldots < \lambda_N$ are the N eigenvalues of the Jacobian $\frac{\partial f}{\partial u}$, and $C(u^-_{j+\frac{1}{2}}, u^+_{j+\frac{1}{2}})$ is the curve in the phase space that connects $u^-_{j+\frac{1}{2}} := p^n_j(x_{j+\frac{1}{2}})$ and $u^+_{j+\frac{1}{2}} := p^n_{j+1}(x_{j+\frac{1}{2}})$.

For example, in the genuinely nonlinear or linearly degenerate case, we have

$$\begin{aligned} a^+_{j+\frac{1}{2}} &= \max\left\{\lambda_N\Big(\frac{\partial f}{\partial u}(u^-_{j+\frac{1}{2}})\Big),\lambda_N\Big(\frac{\partial f}{\partial u}(u^+_{j+\frac{1}{2}})\Big),0\right\}, \\ a^-_{j+\frac{1}{2}} &= \min\left\{\lambda_1\Big(\frac{\partial f}{\partial u}(u^-_{j+\frac{1}{2}})\Big),\lambda_1\Big(\frac{\partial f}{\partial u}(u^+_{j+\frac{1}{2}})\Big),0\right\}, \end{aligned} \tag{3.1}$$

In fact, these one-sided local speeds are related to the CFL number. Note that in the schemes from [26, 24] only the spectral radius of $\frac{\partial f}{\partial u}$ is used, and for its computation one actually needs to know both λ_1 and λ_N.

Further, we utilize these one-sided local speeds of propagation in the following way. We consider the non-equal rectangular domains

$$[x^n_{j-\frac{1}{2},r}, x^n_{j+\frac{1}{2},l}] \times [t^n, t^{n+1}] \quad \text{and} \quad [x^n_{j+\frac{1}{2},l}, x^n_{j+\frac{1}{2},r}] \times [t^n, t^{n+1}], \tag{3.2}$$

with $x^n_{j+\frac{1}{2},l} := x_{j+\frac{1}{2}} + \Delta t a^-_{j+\frac{1}{2}}$, and $x^n_{j+\frac{1}{2},r} := x_{j+\frac{1}{2}} + \Delta t a^+_{j+\frac{1}{2}}$, where the solution of (1.1) with the initial data $\widetilde{u}(x,t^n)$ is smooth and nonsmooth, respectively.

The cell averages

$$\bar{w}^{n+1}_j = \frac{1}{x^n_{j+\frac{1}{2},l} - x^n_{j-\frac{1}{2},r}}\left[\int\limits_{x^n_{j-\frac{1}{2},r}}^{x^n_{j+\frac{1}{2},l}} p^n_j(x)\,dx - \int\limits_{t^n}^{t^{n+1}} \Big(f(u(x^n_{j+\frac{1}{2},l},t)) - f(u(x^n_{j-\frac{1}{2},r},t))\Big)\,dt\right], \tag{3.3}$$

and

$$\bar{w}^{n+1}_{j+\frac{1}{2}} = \frac{1}{x^n_{j+\frac{1}{2},r} - x^n_{j+\frac{1}{2},l}} \Bigg[\int\limits_{x^n_{j+\frac{1}{2},l}}^{x_{j+\frac{1}{2}}} p^n_j(x)\,dx \;+ \int\limits_{x_{j+\frac{1}{2}}}^{x^n_{j+\frac{1}{2},r}} p^n_{j+1}(x)\,dx - \\ - \int\limits_{t^n}^{t^{n+1}} \Big(f(u(x^n_{j+\frac{1}{2},r},t)) - f(u(x^n_{j+\frac{1}{2},l},t)) \Big)\,dt \Bigg] \tag{3.4}$$

are obtained by integrating (1.1) over the corresponding domains in (3.2), see Figure 3.1.

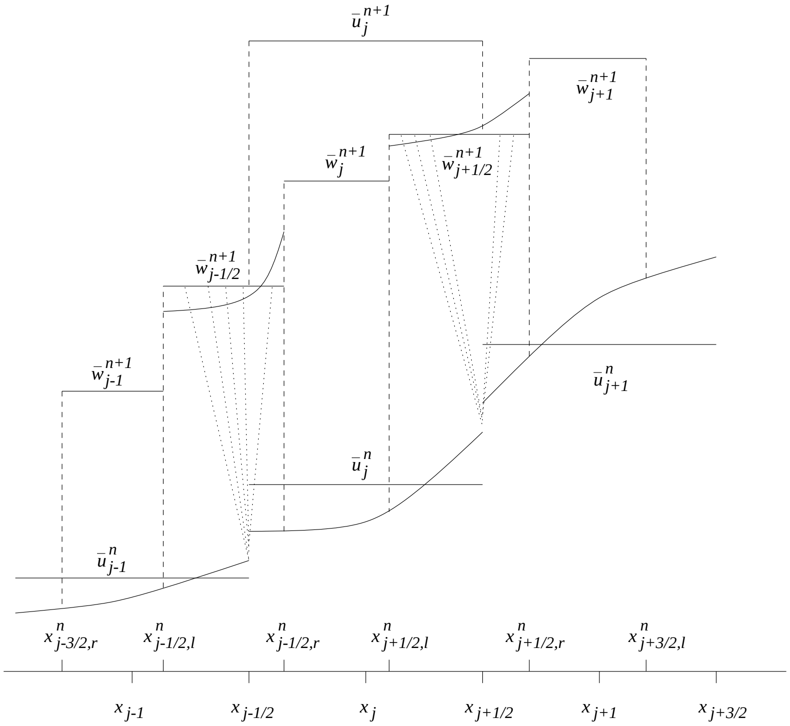

Figure 3.1: Central-upwind differencing

Given the polynomials $\{p^n_j\}$, the spatial integrals in (3.3) and (3.4) can be computed explicitly. To discretize the flux integrals there, one may use an appropriate quadrature formula, since the solution is smooth along the line segments $(x^n_{j+\frac{1}{2},l}, t)$, $t^n \le t < t^{n+1}$ and $(x^n_{j+\frac{1}{2},r}, t)$, $t^n \le t < t^{n+1}$.

Further, we build a new piecewise polynomial reconstruction

$$\widetilde{w}^{n+1}(x) = \sum_j \Big(\widetilde{w}^{n+1}_j(x)\chi_{[x^n_{j-\frac{1}{2},r},\, x^n_{j+\frac{1}{2},l}]} + \widetilde{w}^{n+1}_{j+\frac{1}{2}}(x)\chi_{[x^n_{j+\frac{1}{2},l},\, x^n_{j+\frac{1}{2},r}]} \Big),$$

where the χ's are the characteristic functions of the corresponding intervals. The construction of our scheme is then completed by projecting $\widetilde{w}^{n+1}$ back onto the original grid, namely we compute the cell averages

$$\bar{u}^{n+1}_j = \frac{1}{\Delta x} \int\limits_{x_{j-\frac{1}{2}}}^{x_{j+\frac{1}{2}}} \widetilde{w}^{n+1}(x)\,dx \tag{3.5}$$

at the next time level. This leads to a fully-discrete Godunov-type central-upwind scheme, which can be derived explicitly. Its derivation is similar to the derivation of the central schemes from [26, 24]. We omit here the details of these rather messy computations and continue within a much simpler semi-discrete framework.

The time derivative of $\bar{u}_j(t)$ is expressed with the help of (3.5) as

$$\frac{d}{dt}\bar{u}_j(t) = \lim_{\Delta t\to 0}\frac{\bar{u}_j^{n+1}-\bar{u}_j^n}{\Delta t} = \lim_{\Delta t\to 0}\frac{1}{\Delta t}\left[\frac{1}{\Delta x}\int\limits_{x_{j-\frac{1}{2}}}^{x_{j+\frac{1}{2}}}\widetilde{w}^{n+1}(x)\,dx - \bar{u}_j^n\right]. \tag{3.6}$$

Now, let us suppose that the slopes of $\widetilde{w}^{n+1}_{j\pm\frac{1}{2}}$ are uniformly bounded, independently of Δt. Since the width of the Riemann fans is bounded by $(a^+_{j+\frac{1}{2}} - a^-_{j+\frac{1}{2}})\Delta t$, we obtain

$$\widetilde{w}^{n+1}_{j\pm\frac{1}{2}}(x) = \bar{w}^{n+1}_{j\pm\frac{1}{2}} + \mathcal{O}(\Delta t), \qquad \forall x\in[x^n_{j\pm\frac{1}{2},l},\, x^n_{j\pm\frac{1}{2},r}]. \tag{3.7}$$

¿From the conservation property of the reconstruction we have

$$\frac{1}{(x^n_{j+\frac{1}{2},l} - x^n_{j-\frac{1}{2},r})}\int\limits_{x^n_{j-\frac{1}{2},r}}^{x^n_{j+\frac{1}{2},l}}\widetilde{w}^{n+1}_j(x)\,dx = \bar{w}^{n+1}_j. \tag{3.8}$$

Substituting (3.7) and (3.8) in (3.6) results in

$$\frac{d}{dt}\bar{u}_j(t) = \lim_{\Delta t\to 0}\frac{1}{\Delta t}\Big(\frac{x^n_{j-\frac{1}{2},r} - x_{j-\frac{1}{2}}}{\Delta x}\bar{w}^{n+1}_{j-\frac{1}{2}} + \frac{x^n_{j+\frac{1}{2},l} - x^n_{j-\frac{1}{2},r}}{\Delta x}\bar{w}^{n+1}_j - \bar{u}^n_j + \frac{x_{j+\frac{1}{2}} - x^n_{j+\frac{1}{2},l}}{\Delta x}\bar{w}^{n+1}_{j+\frac{1}{2}}\Big). \tag{3.9}$$

Using the definition of $x^n_{j-\frac{1}{2},r}$, $x^n_{j+\frac{1}{2},l}$ in (3.9) yields

$$\frac{d}{dt}\bar{u}_j(t) = \frac{a^+_{j-\frac{1}{2}}}{\Delta x}\lim_{\Delta t\to 0}\bar{w}^{n+1}_{j-\frac{1}{2}} + \lim_{\Delta t\to 0}\frac{1}{\Delta t}\left(\frac{x^n_{j+\frac{1}{2},l} - x^n_{j-\frac{1}{2},r}}{\Delta x}\bar{w}^{n+1}_j - \bar{u}^n_j\right) - \frac{a^-_{j+\frac{1}{2}}}{\Delta x}\lim_{\Delta t\to 0}\bar{w}^{n+1}_{j+\frac{1}{2}}. \tag{3.10}$$

The three limits in (3.10) are computed separately. ¿From (3.3) and (3.4) we obtain

$$\lim_{\Delta t\to 0}\frac{1}{\Delta t}\left(\frac{x^n_{j+\frac{1}{2},l} - x^n_{j-\frac{1}{2},r}}{\Delta x}\bar{w}^{n+1}_j - \bar{u}^n_j\right) = \frac{a^-_{j+\frac{1}{2}}u^-_{j+\frac{1}{2}} - a^+_{j-\frac{1}{2}}u^+_{j-\frac{1}{2}}}{\Delta x} - \frac{f(u^-_{j+\frac{1}{2}}) - f(u^+_{j-\frac{1}{2}})}{\Delta x}, \tag{3.11}$$

and

$$\lim_{\Delta t\to 0}\bar{w}^{n+1}_{j+\frac{1}{2}} = \frac{a^+_{j+\frac{1}{2}}u^+_{j+\frac{1}{2}} - a^-_{j+\frac{1}{2}}u^-_{j+\frac{1}{2}}}{a^+_{j+\frac{1}{2}} - a^-_{j+\frac{1}{2}}} - \frac{f(u^+_{j+\frac{1}{2}}) - f(u^-_{j+\frac{1}{2}})}{a^+_{j+\frac{1}{2}} - a^-_{j+\frac{1}{2}}}, \tag{3.12}$$

where

$$u^+_{j+\frac{1}{2}} := p_{j+1}(x_{j+\frac{1}{2}}), \quad \text{and} \quad u^-_{j+\frac{1}{2}} := p_j(x_{j+\frac{1}{2}}) \tag{3.13}$$

stand for the corresponding right and left values of the piecewise polynomial interpolant $\{p_j\}$, reconstructed at time t.

Finally, a substitution of (3.11) and (3.12) in (3.10) results in our new semi-discrete *central-upwind* scheme, which can be written in the following conservative form,

$$\frac{d}{dt}\bar{u}_j(t) = -\frac{H_{j+\frac{1}{2}}(t) - H_{j-\frac{1}{2}}(t)}{\Delta x}. \tag{3.14}$$

Here, the numerical fluxes $H_{j+\frac{1}{2}}$ are given by

$$H_{j+\frac{1}{2}}(t) := \frac{a^+_{j+\frac{1}{2}} f(u^-_{j+\frac{1}{2}}) - a^-_{j+\frac{1}{2}} f(u^+_{j+\frac{1}{2}})}{a^+_{j+\frac{1}{2}} - a^-_{j+\frac{1}{2}}} + \frac{a^+_{j+\frac{1}{2}} a^-_{j+\frac{1}{2}}}{a^+_{j+\frac{1}{2}} - a^-_{j+\frac{1}{2}}} \left[u^+_{j+\frac{1}{2}} - u^-_{j+\frac{1}{2}} \right]. \tag{3.15}$$

Remarks.

1. The new semi-discrete scheme (3.13)–(3.15) is a Godunov-type central scheme, since it is based on integration over Riemann fans. It does not require characteristic decompositions and Riemann solvers, and therefore it preserves the main advantage of the central schemes – simplicity.

2. Like in the semi-discrete schemes, proposed in [26], the numerical viscosity of (3.13)–(3.15) is independent of $\mathcal{O}(1/\Delta t)$, and thus it can be used for steady state computations. Moreover, due to a more accurate estimate of the widths of the Riemann fans, the numerical dissipation in (3.13)–(3.15) is even smaller than the numerical viscosity of the schemes from [26, 24]. Notice that if one takes

$$a^+_{j+\frac{1}{2}} = -a^-_{j+\frac{1}{2}} = a_{j+\frac{1}{2}} := \max_{\omega \in C(u^{n-}_{j+\frac{1}{2}}, u^{n+}_{j+\frac{1}{2}})} \rho\Big(\frac{\partial f}{\partial u}(\omega)\Big),$$

then the numerical flux (3.15) reduces to

$$H_{j+\frac{1}{2}}(t) := \frac{f(u^+_{j+\frac{1}{2}}) + f(u^-_{j+\frac{1}{2}})}{2} - \frac{a_{j+\frac{1}{2}}}{2} \left[u^+_{j+\frac{1}{2}} - u^-_{j+\frac{1}{2}} \right],$$

which is the numerical flux of the schemes from [26, 24].

3. We would like to point out, that the first-order version of our scheme is exactly the semi-discrete version of the scheme in [17, 12], namely

$$\begin{aligned}\dot{u}_j(t) = &-\frac{1}{\Delta x}\left(- f(u^n_{j-1}) \frac{a^+_{j-\frac{1}{2}}}{a^+_{j-\frac{1}{2}} - a^-_{j-\frac{1}{2}}} + f(u^n_j) \frac{a^+_{j+\frac{1}{2}} a^+_{j-\frac{1}{2}} - a^-_{j-\frac{1}{2}} a^-_{j+\frac{1}{2}}}{(a^+_{j-\frac{1}{2}} - a^-_{j-\frac{1}{2}})(a^+_{j+\frac{1}{2}} - a^-_{j+\frac{1}{2}})} - f(u^n_{j+1}) \frac{a^-_{j+\frac{1}{2}}}{a^+_{j+\frac{1}{2}} - a^-_{j+\frac{1}{2}}} \right) - \\ &-\frac{1}{\Delta x}\left(u^n_{j-1} \frac{a^+_{j-\frac{1}{2}} a^-_{j-\frac{1}{2}}}{a^+_{j-\frac{1}{2}} - a^-_{j-\frac{1}{2}}} - u^n_j \left(\frac{a^+_{j+\frac{1}{2}} a^-_{j+\frac{1}{2}}}{a^+_{j+\frac{1}{2}} - a^-_{j+\frac{1}{2}}} - \frac{a^+_{j-\frac{1}{2}} a^-_{j-\frac{1}{2}}}{a^+_{j-\frac{1}{2}} - a^-_{j-\frac{1}{2}}} \right) + u^n_{j+1} \frac{a^+_{j+\frac{1}{2}} a^-_{j+\frac{1}{2}}}{a^+_{j+\frac{1}{2}} - a^-_{j+\frac{1}{2}}} \right)\end{aligned} \tag{3.16}$$

Moreover, if the flux f is monotone, the first-order central scheme (3.16) reduces to the standard upwind scheme. That is why we call our new schemes *central-upwind*. For example, if $f'(u) \geq 0$, then $a^-_{j+\frac{1}{2}} = 0$ for all j and (3.16) simplifies to

$$\dot{u}_j(t) = -\frac{f(u^n_j) - f(u^n_{j-1})}{\Delta x}.$$

4. A fully discrete, two-dimensional, third order accurate scheme using the Harten-Lax-VanLeer approximate Riemann-solver [17, 12] was implemented and tested in [41].

5. It can be proved that a scalar second-order version of (3.13)–(3.15), together with the minmod reconstruction (2.7), (2.9) is a TVD scheme, that is

$$\|u(\cdot, t)\|_{BV} \leq \|u(\cdot, 0)\|_{BV}.$$

The proof is analogous to the proof of Theorem 4.1 in [26], and we leave the details to the reader.

6. The semi-discrete scheme (3.13)–(3.15) is a system of time dependent ODEs, which can be solved by any stable ODE solver which retains the spatial accuracy of the semi-discrete scheme. In the numerical examples below, we have used the TVD Runge-Kutta method, proposed in [47, 45].

7. The scheme (3.13)–(3.15) can be easily generalized and applied to convection-diffusion equations in a straightforward manner. For details, we refer the reader to [26, 24].

3.2 Semi-discrete central-upwind schemes for multidimensional conservation laws

The semi-discrete central-upwind schemes, presented in Section 3.1, can be generalized to the multidimensional case. Without loss of generality, we consider the two-dimensional system

$$u_t + f(u)_x + g(u)_y = 0. \tag{3.17}$$

Given the grid points $x_j := j\Delta x$, $y_k := k\Delta y$ and the intermediate points $x_{j\pm\frac{1}{2}} := x_j \pm \frac{\Delta x}{2}$, $y_{k\pm\frac{1}{2}} := y_k \pm \frac{\Delta y}{2}$, we start at time $t = t^n$ with a conservative piecewise polynomial reconstruction of an appropriate order

$$\widetilde{u}^n(x,y) := \sum_{j,k} p^n_{j,k}(x,y)\chi_{j,k},$$

where $\chi_{j,k}$ is the characteristic function of the cell $[x_{j-\frac{1}{2}}, x_{j+\frac{1}{2}}] \times [y_{k-\frac{1}{2}}, y_{k+\frac{1}{2}}]$. In the numerical examples in this paper, we have used the third-order piecewise quadratic reconstruction, briefly described in Section 4.

We use the notation

$$\begin{aligned}
&u_{j,k} := p^n_{j,k}(x_j, y_k), \quad u^{\mathrm{N}}_{j,k} := p^n_{j,k}(x_j, y_{k+\frac{1}{2}}), \quad u^{\mathrm{S}}_{j,k} := p^n_{j,k}(x_j, y_{k-\frac{1}{2}}),\\
&u^{\mathrm{E}}_{j,k} := p^n_{j,k}(x_{j+\frac{1}{2}}, y_k), \quad u^{\mathrm{W}}_{j,k} := p^n_{j,k}(x_{j-\frac{1}{2}}, y_k), \quad u^{\mathrm{NE}}_{j,k} := p^n_{j,k}(x_{j+\frac{1}{2}}, y_{k+\frac{1}{2}}),\\
&u^{\mathrm{NW}}_{j,k} := p^n_{j,k}(x_{j-\frac{1}{2}}, y_{k+\frac{1}{2}}), \quad u^{\mathrm{SE}}_{j,k} := p^n_{j,k}(x_{j+\frac{1}{2}}, y_{k-\frac{1}{2}}), \quad u^{\mathrm{SW}}_{j,k} := p^n_{j,k}(x_{j-\frac{1}{2}}, y_{k-\frac{1}{2}}),
\end{aligned} \tag{3.18}$$

for the corresponding point values, and

$$\bar{u}_{j,k} := \frac{1}{\Delta x \Delta y} \int\limits_{x_{j-\frac{1}{2}}}^{x_{j+\frac{1}{2}}} \int\limits_{y_{k-\frac{1}{2}}}^{y_{k+\frac{1}{2}}} p^n_{j,k}(x,y)\,dxdy$$

for the cell averages.

The piecewise polynomial interpolant $\widetilde{u}^n$ may have discontinuities along the lines $x = x_{j\pm\frac{1}{2}}$ and $y = y_{k\pm\frac{1}{2}}$, which propagate with different right- and left-sided local speeds. To estimate them is a non-trivial problem, but in practice one may use

$$\begin{aligned}
a^+_{j+\frac{1}{2},k} &:= \max\Big\{\lambda_N\Big(\frac{\partial f}{\partial u}(u^{\mathrm{W}}_{j+1,k})\Big), \lambda_N\Big(\frac{\partial f}{\partial u}(u^{\mathrm{E}}_{j,k})\Big), 0\Big\},\\
b^+_{j,k+\frac{1}{2}} &:= \max\Big\{\lambda_N\Big(\frac{\partial g}{\partial u}(u^{\mathrm{S}}_{j,k+1})\Big), \lambda_N\Big(\frac{\partial g}{\partial u}(u^{\mathrm{N}}_{j,k})\Big), 0\Big\},\\
a^-_{j+\frac{1}{2},k} &:= \min\Big\{\lambda_1\Big(\frac{\partial f}{\partial u}(u^{\mathrm{W}}_{j+1,k})\Big), \lambda_1\Big(\frac{\partial f}{\partial u}(u^{\mathrm{E}}_{j,k})\Big), 0\Big\},\\
b^-_{j,k+\frac{1}{2}} &:= \min\Big\{\lambda_1\Big(\frac{\partial g}{\partial u}(u^{\mathrm{S}}_{j,k+1})\Big), \lambda_1\Big(\frac{\partial g}{\partial u}(u^{\mathrm{N}}_{j,k})\Big), 0\Big\},
\end{aligned} \tag{3.19}$$

respectively. As in [25], we consider the nonuniform domains

$$D_{j,k} \times [t^n, t^{n+1}], \quad D_{j\pm\frac{1}{2},k} \times [t^n, t^{n+1}], \quad D_{j,k\pm\frac{1}{2}} \times [t^n, t^{n+1}], \quad D_{j\pm\frac{1}{2},k\pm\frac{1}{2}} \times [t^n, t^{n+1}].$$

The D's are outlined in Figure 3.2 and defined by

$$D_{j,k+\frac{1}{2}} := [x_{j-\frac{1}{2}} + A^+_{j-\frac{1}{2},k+\frac{1}{2}}\Delta t,\ x_{j+\frac{1}{2}} + A^-_{j+\frac{1}{2},k+\frac{1}{2}}\Delta t] \times [y_{k+\frac{1}{2}} + b^-_{j,k+\frac{1}{2}}\Delta t,\ y_{k+\frac{1}{2}} + b^+_{j,k+\frac{1}{2}}\Delta t],$$

$$D_{j+\frac12,k} := [x_{j+\frac12} + a^-_{j+\frac12,k}\Delta t,\ x_{j+\frac12} + a^+_{j+\frac12,k}\Delta t] \times [y_{k-\frac12} + B^+_{j+\frac12,k-\frac12}\Delta t,\ y_{k+\frac12} + B^-_{j+\frac12,k+\frac12}\Delta t],$$

$$D_{j+\frac12,k+\frac12} := [x_{j+\frac12} + A^-_{j+\frac12,k+\frac12}\Delta t,\ x_{j+\frac12} + A^+_{j+\frac12,k+\frac12}\Delta t] \times [y_{k+\frac12} + B^-_{j+\frac12,k+\frac12}\Delta t,\ y_{k+\frac12} + B^+_{j+\frac12,k+\frac12}\Delta t],$$

$$D_{j,k} := [x_{j-\frac12},\ x_{j+\frac12}] \times [y_{k-\frac12},\ y_{k+\frac12}] \setminus \bigcup_{\pm} [D_{j,k\pm\frac12} \cup D_{j\pm\frac12,k} \cup D_{j\pm\frac12,k\pm\frac12}],$$

where

$$A^+_{j+\frac12,k+\frac12} := \max\left\{a^+_{j+\frac12,k}, a^+_{j+\frac12,k+1}\right\}, \qquad B^+_{j+\frac12,k+\frac12} := \max\left\{b^+_{j,k+\frac12}, b^+_{j+1,k+\frac12}\right\},$$

$$A^-_{j+\frac12,k+\frac12} := \min\left\{a^-_{j+\frac12,k}, a^-_{j+\frac12,k+1}\right\}, \qquad B^-_{j+\frac12,k+\frac12} := \min\left\{b^-_{j,k+\frac12}, b^-_{j+1,k+\frac12}\right\}.$$

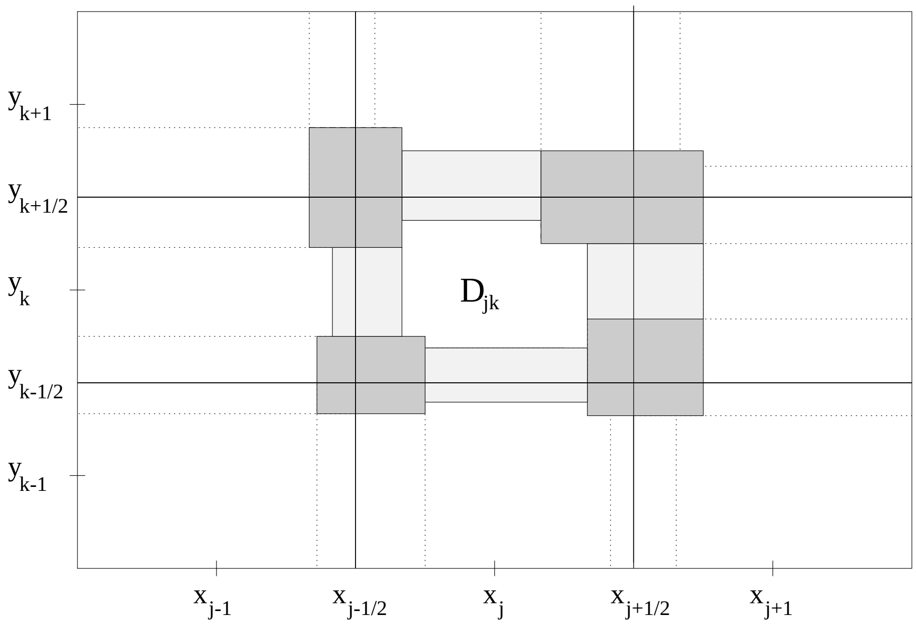

Figure 3.2: Two-dimensional central-upwind differencing

Similarly to the one-dimensional case, under an appropriate CFL condition, the solution of system (3.17) with initial data $\widetilde{u}(x,y)$ is smooth in the domain $D_{j,k}$, and may be nonsmooth in the other domains. Notice that, in general, $D_{j,k}$ is a nonrectangular domain inside the (j,k)-cell, see Figure 3.2.

An integration of the system (3.17) over the D's results in new cell averages $\{\bar{w}^{n+1}_{j,k+\frac12}\}$, $\{\bar{w}^{n+1}_{j+\frac12,k}\}$, $\{\bar{w}^{n+1}_{j+\frac12,k+\frac12}\}$, and $\{\bar{w}^{n+1}_{j,k}\}$. They are

$$\bar{w}^{n+1}_{j,k+\frac12} = \frac{1}{|D_{j,k+\frac12}|}\Bigg(\iint\limits_{D_{j,k+\frac12}} \widetilde{u}^n(x,y)\,dx\,dy -$$

$$- \int\limits_{t^n}^{t^{n+1}} \int\limits_{y_{k+\frac12}+b^-_{j,k+\frac12}\Delta t}^{y_{k+\frac12}+b^+_{j,k+\frac12}\Delta t} f(u(x,y,t))\Bigg|_{x=x_{j-\frac12}+A^+_{j-\frac12,k+\frac12}\Delta t}^{x_{j+\frac12}+A^-_{j+\frac12,k+\frac12}\Delta t} dy\,dt -$$

$$
- \int\limits_{t^n}^{t^{n+1}} \int\limits_{x_{j-\frac{1}{2}}+A^+_{j-\frac{1}{2},k+\frac{1}{2}}\Delta t}^{x_{j+\frac{1}{2}}+A^-_{j+\frac{1}{2},k+\frac{1}{2}}\Delta t} g(u(x,y,t))\Bigg|_{y=y_{k+\frac{1}{2}}+b^-_{j,k+\frac{1}{2}}\Delta t}^{y_{k+\frac{1}{2}}+b^+_{j,k+\frac{1}{2}}\Delta t} dx\,dt\Bigg), \tag{3.20}
$$

$$
\begin{aligned}
\bar{w}^{n+1}_{j+\frac{1}{2},k} &= \frac{1}{|D_{j+\frac{1}{2},k}|}\Bigg(\iint\limits_{D_{j+\frac{1}{2},k}} \widetilde{u}^n(x,y)\,dx\,dy - \\
&- \int\limits_{t^n}^{t^{n+1}} \int\limits_{y_{k-\frac{1}{2}}+B^+_{j+\frac{1}{2},k-\frac{1}{2}}\Delta t}^{y_{k+\frac{1}{2}}+B^-_{j+\frac{1}{2},k+\frac{1}{2}}\Delta t} f(u(x,y,t))\Bigg|_{x=x_{j+\frac{1}{2}}+a^-_{j+\frac{1}{2},k}\Delta t}^{x_{j+\frac{1}{2}}+a^+_{j+\frac{1}{2},k}\Delta t} dy\,dt - \\
&- \int\limits_{t^n}^{t^{n+1}} \int\limits_{x_{j+\frac{1}{2}}+a^-_{j+\frac{1}{2},k}\Delta t}^{x_{j+\frac{1}{2}}+a^+_{j+\frac{1}{2},k}\Delta t} g(u(x,y,t))\Bigg|_{y=y_{k-\frac{1}{2}}+B^+_{j+\frac{1}{2},k-\frac{1}{2}}\Delta t}^{y_{k+\frac{1}{2}}+B^-_{j+\frac{1}{2},k+\frac{1}{2}}\Delta t} dx\,dt\Bigg),
\end{aligned} \tag{3.21}
$$

$$
\begin{aligned}
\bar{w}^{n+1}_{j+\frac{1}{2},k+\frac{1}{2}} &= \frac{1}{|D_{j+\frac{1}{2},k+\frac{1}{2}}|}\Bigg(\iint\limits_{D_{j+\frac{1}{2},k+\frac{1}{2}}} \widetilde{u}^n(x,y)\,dx\,dy - \\
&- \int\limits_{t^n}^{t^{n+1}} \int\limits_{y_{k+\frac{1}{2}}+B^-_{j+\frac{1}{2},k+\frac{1}{2}}\Delta t}^{y_{k+\frac{1}{2}}+B^+_{j+\frac{1}{2},k+\frac{1}{2}}\Delta t} f(u(x,y,t))\Bigg|_{x=x_{j+\frac{1}{2}}+A^-_{j+\frac{1}{2},k+\frac{1}{2}}\Delta t}^{x_{j+\frac{1}{2}}+A^+_{j+\frac{1}{2},k+\frac{1}{2}}\Delta t} dy\,dt - \\
&- \int\limits_{t^n}^{t^{n+1}} \int\limits_{x_{j+\frac{1}{2}}+A^-_{j+\frac{1}{2},k+\frac{1}{2}}\Delta t}^{x_{j+\frac{1}{2}}+A^+_{j+\frac{1}{2},k+\frac{1}{2}}\Delta t} g(u(x,y,t))\Bigg|_{y=y_{k+\frac{1}{2}}+B^-_{j+\frac{1}{2},k+\frac{1}{2}}\Delta t}^{y_{k+\frac{1}{2}}+B^+_{j+\frac{1}{2},k+\frac{1}{2}}\Delta t} dx\,dt\Bigg).
\end{aligned} \tag{3.22}
$$

The average $\bar{w}^{n+1}_{j,k}$ can be computed in a similar way. Further, the spatial integrals in (3.20)–(3.22) can be evaluated exactly, and the flux integrals can be discretized by an appropriate quadrature formula (applying the technique used in [4, 19, 31, 34]).

Now, the above cell averages are used for an intermediate piecewise polynomial reconstruction

$$
\widetilde{w}^{n+1}(x,y) := \sum_{j,k}\left[\bar{w}^{n+1}_{j,k}\widetilde{\chi}_{j,k} + \bar{w}^{n+1}_{j+\frac{1}{2},k}\widetilde{\chi}_{j+\frac{1}{2},k} + \bar{w}^{n+1}_{j,k+\frac{1}{2}}\widetilde{\chi}_{j,k+\frac{1}{2}} + \bar{w}^{n+1}_{j+\frac{1}{2},k+\frac{1}{2}}\widetilde{\chi}_{j+\frac{1}{2},k+\frac{1}{2}}\right], \tag{3.23}
$$

which is then projected back onto the original cells (the notation $\widetilde{\chi}$ is used for the characteristic functions of the domains D). As in the one-dimensional case, we assume that the spatial derivatives of $\widetilde{w}^{n+1}$ are bounded independently of Δt. The construction of our fully-discrete central-upwind scheme is thus completed by the computation of the cell averages at the next time level $t = t^{n+1}$,

$$
\bar{u}^{n+1}_{j,k} = \frac{1}{\Delta x \Delta y} \int\limits_{x_{j-\frac{1}{2}}}^{x_{j+\frac{1}{2}}} \int\limits_{y_{k-\frac{1}{2}}}^{y_{k+\frac{1}{2}}} \widetilde{w}^{n+1}(x,y)\,dxdy. \tag{3.24}
$$

The derivation of the explicit form of the fully-discrete higher-order scheme is omitted, since it is rather complicated and is of no practical use. Note, however, that Wendroff [50] has recently proposed a two-dimensional version of the Harten-Lax-Leer Riemann-solver, which is closely related to the first-order fully-discrete version of our scheme.

As in [25, Section 3.3], we continue within the semi-discrete framework (as $\Delta t \to 0$), where all the computations are much simpler.

We use the following notation for the intersections of the cell $[x_{j-\frac{1}{2}}, x_{j+\frac{1}{2}}] \times [y_{k-\frac{1}{2}}, y_{k+\frac{1}{2}}]$ with the domains $D - C_{j\pm\frac{1}{2},k\pm\frac{1}{2}}$ for the four corners, $S_{j\pm\frac{1}{2},k}$, $S_{j,k\pm\frac{1}{2}}$ for the four side domains and $D_{j,k}$ for the center. In these domains, since $|C| \sim (\Delta t)^2$ and $|S| \sim \Delta t$, the relation between $\widetilde{w}^{n+1}$ and $\bar{w}^{n+1}$ is given by

$$\iint\limits_{C_{j\pm\frac{1}{2},k\pm\frac{1}{2}}} \widetilde{w}^{n+1}_{j\pm\frac{1}{2},k\pm\frac{1}{2}}\, dxdy = \mathcal{O}((\Delta t)^2), \tag{3.25}$$

$$\iint\limits_{S_{j\pm\frac{1}{2},k}} \widetilde{w}^{n+1}_{j\pm\frac{1}{2},k}\, dxdy = |S_{j\pm\frac{1}{2},k}|\; \bar{w}^{n+1}_{j\pm\frac{1}{2},k} + \mathcal{O}(\Delta t^2), \tag{3.26}$$

$$\iint\limits_{S_{j,k\pm\frac{1}{2}}} \widetilde{w}^{n+1}_{j,k\pm\frac{1}{2}}\, dxdy = |S_{j,k\pm\frac{1}{2}}|\; \bar{w}^{n+1}_{j,k\pm\frac{1}{2}} + \mathcal{O}(\Delta t^2). \tag{3.27}$$

Also, the conservation property of the reconstruction $\widetilde{w}^{n+1}$ yields

$$\iint\limits_{D_{j,k}} \widetilde{w}^{n+1}_{j,k}(x,y)\, dxdy = |D_{j,k}|\bar{w}^{n+1}_{j,k}. \tag{3.28}$$

We now use (3.24) together with (3.25)–(3.28), and obtain

$$\begin{aligned}
\frac{d}{dt}\bar{u}_{j,k}(t) &= \lim_{\Delta t\to 0}\frac{\bar{u}^{n+1}_{j,k}-\bar{u}^{n}_{j,k}}{\Delta t} = \lim_{\Delta t\to 0}\frac{1}{\Delta t\Delta x\Delta y}\Bigg(\sum_{\pm}\iint\limits_{C_{j\pm\frac{1}{2},k\pm\frac{1}{2}}} \widetilde{w}^{n+1}_{j\pm\frac{1}{2},k\pm\frac{1}{2}}\, dxdy + \\
&+\sum_{\pm}\iint\limits_{S_{j,k\pm\frac{1}{2}}} \widetilde{w}^{n+1}_{j,k\pm\frac{1}{2}}\, dxdy + \sum_{\pm}\iint\limits_{S_{j\pm\frac{1}{2},k}} \widetilde{w}^{n+1}_{j\pm\frac{1}{2},k}\, dxdy + \iint\limits_{D_{j,k}} \widetilde{w}^{n+1}_{j,k}\, dxdy - \Delta x\Delta y\; \bar{u}^{n}_{j,k}\Bigg) = \\
&= \lim_{\Delta t\to 0}\left(\sum_{\pm}\frac{|S_{j,k\pm\frac{1}{2}}|}{\Delta t\Delta x\Delta y}\bar{w}^{n+1}_{j,k\pm\frac{1}{2}} + \sum_{\pm}\frac{|S_{j\pm\frac{1}{2},k}|}{\Delta t\Delta x\Delta y}\bar{w}^{n+1}_{j\pm\frac{1}{2},k}\right) + \lim_{\Delta t\to 0}\frac{1}{\Delta t}\left[\frac{|D_{j,k}|}{\Delta x\Delta y}\bar{w}^{n+1}_{j,k} - \bar{u}^{n}_{j,k}\right].
\end{aligned} \tag{3.29}$$

For the first sum on the RHS, we use the fact that $|S_{j,k\pm\frac{1}{2}}| = \mp b^{\mp}_{j,k\pm\frac{1}{2}}\Delta t\Delta x + \mathcal{O}((\Delta t)^2)$, which gives

$$\lim_{\Delta t\to 0}\frac{|S_{j,k\pm\frac{1}{2}}|}{\Delta t\Delta x\Delta y}\bar{w}^{n+1}_{j,k\pm\frac{1}{2}} = \mp\frac{b^{\mp}_{j,k\pm\frac{1}{2}}}{\Delta y}\lim_{\Delta t\to 0}\bar{w}^{n+1}_{j,k\pm\frac{1}{2}}. \tag{3.30}$$

The value of $\lim\limits_{\Delta t\to 0}\bar{w}^{n+1}_{j,k\pm\frac{1}{2}}$ is computed from (3.20) and is

$$\pm\frac{b^{\pm}_{j,k\pm\frac{1}{2}}}{(b^{+}_{j,k\pm\frac{1}{2}}-b^{-}_{j,k\pm\frac{1}{2}})\Delta x}\int\limits_{x_{j-\frac{1}{2}}}^{x_{j+\frac{1}{2}}} p^{n}_{j,k\pm 1}(x,y_{k\pm\frac{1}{2}})\, dx \mp \frac{b^{\mp}_{j,k\pm\frac{1}{2}}}{(b^{+}_{j,k\pm\frac{1}{2}}-b^{-}_{j,k\pm\frac{1}{2}})\Delta x}\int\limits_{x_{j-\frac{1}{2}}}^{x_{j+\frac{1}{2}}} p^{n}_{j,k}(x,y_{k\pm\frac{1}{2}})\, dx \mp$$

$$\mp\frac{1}{(b^+_{j,k\pm\frac12}-b^-_{j,k\pm\frac12})\Delta x}\int\limits_{x_{j-\frac12}}^{x_{j+\frac12}}\Big\{g(p^n_{j,k\pm1}(x,y_{k\pm\frac12}))-g(p^n_{j,k}(x,y_{k\pm\frac12}))\Big\}\,dx. \tag{3.31}$$

We then apply Simpson's quadrature formula to the above integrals, and using (3.30), we arrive at

$$\begin{aligned}\lim_{\Delta t\to 0}\frac{|S_{j,k\pm\frac12}|}{\Delta t\Delta x\Delta y}\bar w^{n+1}_{j,k\pm\frac12}&\approx-\frac{b^+_{j,k\pm\frac12}b^-_{j,k\pm\frac12}}{6(b^+_{j,k\pm\frac12}-b^-_{j,k\pm\frac12})\Delta y}\Big[u^{\rm SW(NW)}_{j,k\pm1}+4u^{\rm S(N)}_{j,k\pm1}+u^{\rm SE(NE)}_{j,k\pm1}\Big]+\\
+\frac{(b^\mp_{j,k\pm\frac12})^2}{6(b^+_{j,k\pm\frac12}-b^-_{j,k\pm\frac12})\Delta y}\Big[u^{\rm NW(SW)}_{j,k}+4u^{\rm N(S)}_{j,k}+u^{\rm NE(SE)}_{j,k}\Big]&+\frac{b^\mp_{j,k\pm\frac12}}{6(b^+_{j,k\pm\frac12}-b^-_{j,k\pm\frac12})\Delta y}\Big[g(u^{\rm SW(NW)}_{j,k\pm1})-\\
-g(u^{\rm NW(SW)}_{j,k})+4\Big(g(u^{\rm S(N)}_{j,k\pm1})-g(u^{\rm N(S)}_{j,k})\Big)&+g(u^{\rm SE(NE)}_{j,k\pm1})-g(u^{\rm NE(SE)}_{j,k})\Big]\end{aligned}\tag{3.32}$$

The second sum on the RHS of (3.29) is treated similarly, and we obtain

$$\begin{aligned}\lim_{\Delta t\to 0}\frac{|S_{j\pm\frac12,k}|}{\Delta t\Delta x\Delta y}\bar w^{n+1}_{j\pm\frac12,k}\,dxdy&\approx-\frac{a^+_{j\pm\frac12,k}a^-_{j\pm\frac12,k}}{6(a^+_{j\pm\frac12,k}-a^-_{j\pm\frac12,k})\Delta x}\Big[u^{\rm NW(NE)}_{j\pm1,k}+4u^{\rm W(E)}_{j\pm1,k}+u^{\rm SW(SE)}_{j\pm1,k}\Big]+\\
+\frac{(a^\mp_{j\pm\frac12,k})^2}{6(a^+_{j\pm\frac12,k}-a^-_{j\pm\frac12,k})\Delta x}\Big[u^{\rm NE(NW)}_{j,k}+4u^{\rm E(W)}_{j,k}+u^{\rm SE(SW)}_{j,k}\Big]&+\frac{a^\mp_{j\pm\frac12,k}}{6(a^+_{j\pm\frac12,k}-a^-_{j\pm\frac12,k})\Delta x}\Big[f(u^{\rm NW(NE)}_{j\pm1,k})-\\
-f(u^{\rm NE(NW)}_{j,k})+4\Big(f(u^{\rm W(E)}_{j\pm1,k})-f(u^{\rm E(W)}_{j,k})\Big)&+f(u^{\rm SW(SE)}_{j\pm1,k})-f(u^{\rm SE(SW)}_{j,k})\Big]\end{aligned}\tag{3.33}$$

Finally, we consider the last term on the RHS of (3.29). Since the domain $D_{j,k}$ becomes *rectangular* as $\Delta t\to 0$, up to small corners of a negligible size $\mathcal{O}((\Delta t)^2)$, the integration of (3.17) over $D_{j,k}\times[t^n,t^n+\Delta t]$ and the application of Simpson's rule result in

$$\begin{aligned}&\lim_{\Delta t\to 0}\frac{1}{\Delta t}\left[\frac{|D_{j,k}|}{\Delta x\Delta y}\,\bar w^{n+1}_{j,k}-\bar u^n_{j,k}\right]\approx\\
&\quad\approx\ \frac{a^-_{j+\frac12,k}}{6\Delta x}\Big[u^{\rm NE}_{j,k}+4u^{\rm E}_{j,k}+u^{\rm SE}_{j,k}\Big]-\frac{a^+_{j-\frac12,k}}{6\Delta x}\Big[u^{\rm NW}_{j,k}+4u^{\rm W}_{j,k}+u^{\rm SW}_{j,k}\Big]+\\
&\quad+\ \frac{b^-_{j,k+\frac12}}{6\Delta y}\Big[u^{\rm NW}_{j,k}+4u^{\rm N}_{j,k}+u^{\rm NE}_{j,k}\Big]-\frac{b^+_{j,k-\frac12}}{6\Delta y}\Big[u^{\rm SW}_{j,k}+4u^{\rm S}_{j,k}+u^{\rm SE}_{j,k}\Big]-\\
&\quad-\ \frac{1}{6\Delta x}\Big[f(u^{\rm NE}_{j,k})-f(u^{\rm NW}_{j,k})+4\Big(f(u^{\rm E}_{j,k})-f(u^{\rm W}_{j,k})\Big)+f(u^{\rm SE}_{j,k})-f(u^{\rm SW}_{j,k})\Big]-\\
&\quad-\ \frac{1}{6\Delta y}\Big[g(u^{\rm NW}_{j,k})-g(u^{\rm SW}_{j,k})+4\Big(g(u^{\rm N}_{j,k})-g(u^{\rm S}_{j,k})\Big)+g(u^{\rm NE}_{j,k})-g(u^{\rm SE}_{j,k})\Big].\end{aligned}\tag{3.34}$$

Our two-dimensional semi-discrete central-upwind scheme is obtained by plugging (3.32)–(3.34) into (3.29). It can be written in the following conservative form,

$$\frac{d}{dt}\bar u_{j,k}(t)=-\frac{H^x_{j+\frac12,k}(t)-H^x_{j-\frac12,k}(t)}{\Delta x}-\frac{H^y_{j,k+\frac12}(t)-H^y_{j,k-\frac12}(t)}{\Delta y}, \tag{3.35}$$

where the numerical fluxes are

$$\begin{aligned}
H^x_{j+\frac{1}{2},k} &:= \frac{a^+_{j+\frac{1}{2},k}}{6(a^+_{j+\frac{1}{2},k}-a^-_{j+\frac{1}{2},k})}\Big[f(u^{\rm NE}_{j,k})+4f(u^{\rm E}_{j,k})+f(u^{\rm SE}_{j,k})\Big]- \\
&- \frac{a^-_{j+\frac{1}{2},k}}{6(a^+_{j+\frac{1}{2},k}-a^-_{j+\frac{1}{2},k})}\Big[f(u^{\rm NW}_{j+1,k})+4f(u^{\rm W}_{j+1,k})+f(u^{\rm SW}_{j+1,k})\Big]+ \\
&+ \frac{a^+_{j+\frac{1}{2},k}a^-_{j+\frac{1}{2},k}}{6(a^+_{j+\frac{1}{2},k}-a^-_{j+\frac{1}{2},k})}\Big[u^{\rm NW}_{j+1,k}-u^{\rm NE}_{j,k}+4(u^{\rm W}_{j+1,k}-u^{\rm E}_{j,k})+u^{\rm SW}_{j+1,k}-u^{\rm SE}_{j,k}\Big],
\end{aligned} \tag{3.36}$$

and

$$\begin{aligned}
H^y_{j,k+\frac{1}{2}} &:= \frac{b^+_{j,k+\frac{1}{2}}}{6(b^+_{j,k+\frac{1}{2}}-b^-_{j,k+\frac{1}{2}})}\Big[g(u^{\rm NW}_{j,k})+4g(u^{\rm N}_{j,k})+g(u^{\rm NE}_{j,k})\Big]- \\
&- \frac{b^-_{j,k+\frac{1}{2}}}{6(b^+_{j,k+\frac{1}{2}}-b^-_{j,k+\frac{1}{2}})}\Big[g(u^{\rm SW}_{j,k+1})+4g(u^{\rm S}_{j,k+1})+g(u^{\rm SE}_{j,k+1})\Big]+ \\
&+ \frac{b^+_{j,k+\frac{1}{2}}b^-_{j,k+\frac{1}{2}}}{6(b^+_{j,k+\frac{1}{2}}-b^-_{j,k+\frac{1}{2}})}\Big[u^{\rm SW}_{j,k+1}-u^{\rm NW}_{j,k}+4(u^{\rm S}_{j,k+1}-u^{\rm N}_{j,k})+u^{\rm SE}_{j,k+1}-u^{\rm NE}_{j,k}\Big].
\end{aligned} \tag{3.37}$$

Here, the one-sided local speeds $a^\pm_{j+\frac{1}{2},k}, b^\pm_{j,k+\frac{1}{2}}$ are defined in (3.19), and the values of the u's are computed in (3.18), using the piecewise quadratic reconstruction $\{p_{j,k}\}$ at time t. In our numerical examples, we have implemented the reconstruction introduced in [25] and briefly described in Section 4.

Remarks.

1. Our two-dimensional semi-discrete central upwind scheme (3.35)–(3.37) is a Godunov-type *central* scheme, therefore it can be applied *component-wise* and does not require Riemann solvers. Like in [25], this scheme is constructed as a genuinely multidimensional scheme. Moreover, if one sets

$$a^+_{j+\frac{1}{2},k} := -a^-_{j+\frac{1}{2},k} := \max\left\{a^+_{j+\frac{1}{2},k}, -a^-_{j+\frac{1}{2},k}\right\}, \qquad b^+_{j,k+\frac{1}{2}} := -b^-_{j,k+\frac{1}{2}} := \max\left\{b^+_{j,k+\frac{1}{2}}, -b^-_{j,k+\frac{1}{2}}\right\},$$

the scheme (3.35)–(3.37) reduces to the one in [25].

2. As in the one-dimensional case, our two-dimensional scheme (3.35)–(3.37) has an upwind nature. To illustrate this, let us consider the simplest linear scalar advection equation

$$u_t + au_x + bu_y = 0, \qquad a = \text{const} > 0, \;\; b = \text{const} > 0.$$

In this setting, the first-order version of the scheme (3.35)–(3.37) becomes a standard first-order upwind scheme

$$\frac{d}{dt}u_{j,k}(t) = -a\frac{u_{j,k}-u_{j-1,k}}{\Delta x} - b\frac{u_{j,k}-u_{j,k-1}}{\Delta y}.$$

3. A second-order version of the two-dimensional scheme (3.35)–(3.37) can be obtained if one uses a second-order piecewise polynomial reconstruction (say, the minmod reconstruction) and a lower order midpoint quadrature instead of the fourth-order Simpson's rule. This results in the following scheme,

$$\frac{d}{dt}u_{j,k}(t) = -\frac{H^x_{j+\frac{1}{2},k}(t)-H^x_{j-\frac{1}{2},k}(t)}{\Delta x} - \frac{H^y_{j,k+\frac{1}{2}}(t)-H^y_{j,k-\frac{1}{2}}(t)}{\Delta y}, \tag{3.38}$$

with the corresponding numerical fluxes

$$H^x_{j+\frac{1}{2},k} \quad := \quad \frac{a^+_{j+\frac{1}{2},k} f(u^{\mathrm{E}}_{j,k}) - a^-_{j+\frac{1}{2},k} f(u^{\mathrm{W}}_{j+1,k})}{a^+_{j+\frac{1}{2},k} - a^-_{j+\frac{1}{2},k}} + \frac{a^+_{j+\frac{1}{2},k} a^-_{j+\frac{1}{2},k}}{a^+_{j+\frac{1}{2},k} - a^-_{j+\frac{1}{2},k}} \left[u^{\mathrm{W}}_{j+1,k} - u^{\mathrm{E}}_{j,k} \right], \tag{3.39}$$

and

$$H^y_{j,k+\frac{1}{2}} \quad := \quad \frac{b^+_{j,k+\frac{1}{2}} g(u^{\mathrm{N}}_{j,k}) - b^-_{j,k+\frac{1}{2}} g(u^{\mathrm{S}}_{j,k+1})}{b^+_{j,k+\frac{1}{2}} - b^-_{j,k+\frac{1}{2}}} + \frac{b^+_{j,k+\frac{1}{2}} b^-_{j,k+\frac{1}{2}}}{b^+_{j,k+\frac{1}{2}} - b^-_{j,k+\frac{1}{2}}} \left[u^{\mathrm{S}}_{j,k+1} - u^{\mathrm{N}}_{j,k} \right]. \tag{3.40}$$

The same scheme can be also derived by applying the one-dimensional numerical flux (3.15) in both x- and y-directions (this is the so-called 'dimension-by-dimension' approach, used in [26]).
4. The second-order scheme (3.38)–(3.40) satisfies the *maximum principle*, proved in Section 3.3.
5. The scheme (3.35)–(3.37) can be generalized and applied to convection-diffusion equations (for details see [26, 25, 24]). Also, it can be rather easily extended to the multidimensional case, $d \geq 3$.

3.3 Maximum principle for the two-dimensional second-order central-upwind scheme

In this Section we consider the two-dimensional second-order central upwind scheme (3.38)–(3.40), together with the minmod reconstruction (2.7), (2.9). We solve the time dependent system (3.38), using a TVD Runge-Kutta method. In the next theorem, we prove that under an appropriate CFL condition, the resulting fully-discrete scheme, applied to a scalar conservation law, satisfies the maximum principle, that is

Theorem 3.1 (Maximum Principle) *Consider the scalar conservation laws (3.17). Then the second-order scheme (3.38)–(3.40), with the minmod reconstruction (2.7),(2.9), coupled with a TVD Runge-Kutta method ([47, 45]) satisfies the maximum principle*

$$\min_{j,k}\{u^n_{j,k}\} \leq \min_{j,k}\{u^{n+1}_{j,k}\} \leq \max_{j,k}\{u^{n+1}_{j,k}\} \leq \max_{j,k}\{u^n_{j,k}\}, \tag{3.41}$$

under the CFL condition

$$\max\left(\frac{\Delta t^n}{\Delta x}\max_u |f'(u)|, \frac{\Delta t^n}{\Delta y}\max_u |g'(u)|\right) \leq \frac{1}{8}, \tag{3.42}$$

where Δt^n is the variable time step of the Runge-Kutta method.

Proof: We proceed along the lines of the proof of Theorem 5.1 in [26]. TVD Runge-Kutta methods consist of convex combinations of forward Euler steps. Therefore, it is sufficient to show the maximum principle for the forward Euler time discretization of (3.38), which results in the following fully-discrete scheme,

$$\begin{aligned} u^{n+1}_{j,k} \quad = \quad & u^n_{j,k} - \\ & -\lambda^n \left[\frac{a^+_{j+\frac{1}{2},k} f(u^{\mathrm{E}}_{j,k}) - a^-_{j+\frac{1}{2},k} f(u^{\mathrm{W}}_{j+1,k})}{a^+_{j+\frac{1}{2},k} - a^-_{j+\frac{1}{2},k}} - \frac{a^+_{j-\frac{1}{2},k} f(u^{\mathrm{E}}_{j-1,k}) - a^-_{j-\frac{1}{2},k} f(u^{\mathrm{W}}_{j,k})}{a^+_{j-\frac{1}{2},k} - a^-_{j-\frac{1}{2},k}} \right. \\ & \left. + \frac{a^+_{j+\frac{1}{2},k} a^-_{j+\frac{1}{2},k}}{a^+_{j+\frac{1}{2},k} - a^-_{j+\frac{1}{2},k}} \left\{ u^{\mathrm{W}}_{j+1,k} - u^{\mathrm{E}}_{j,k} \right\} - \frac{a^+_{j-\frac{1}{2},k} a^-_{j-\frac{1}{2},k}}{a^+_{j-\frac{1}{2},k} - a^-_{j-\frac{1}{2},k}} \left\{ u^{\mathrm{W}}_{j,k} - u^{\mathrm{E}}_{j-1,k} \right\} \right] - \end{aligned}$$

$$
-\mu^n \left[\frac{b^+_{j,k+\frac12} g(u^{\rm N}_{j,k}) - b^-_{j,k+\frac12} g(u^{\rm S}_{j,k+1})}{b^+_{j,k+\frac12} - b^-_{j,k+\frac12}} - \frac{b^+_{j,k-\frac12} g(u^{\rm N}_{j,k-1}) - b^-_{j,k-\frac12} g(u^{\rm S}_{j,k})}{b^+_{j,k-\frac12} - b^-_{j,k-\frac12}} \right.
$$
$$
\left. + \frac{b^+_{j,k+\frac12} b^-_{j,k+\frac12}}{b^+_{j,k+\frac12} - b^-_{j,k+\frac12}} \left\{ u^{\rm S}_{j,k+1} - u^{\rm N}_{j,k} \right\} - \frac{b^+_{j,k-\frac12} b^-_{j,k-\frac12}}{b^+_{j,k-\frac12} - b^-_{j,k-\frac12}} \left\{ u^{\rm S}_{j,k} - u^{\rm N}_{j,k-1} \right\} \right], \qquad (3.43)
$$

with $\lambda^n := \Delta t^n/\Delta x$ and $\mu^n := \Delta t^n/\Delta y$. We use the notation

$$
\Delta^x_{j,k} u := u^{\rm E}_{j,k} - u^{\rm W}_{j,k}, \quad \Delta^x_{j+\frac12,k} u := u^{\rm W}_{j+1,k} - u^{\rm E}_{j,k}, \quad \Delta^x_{j-\frac12,k} u := u^{\rm W}_{j,k} - u^{\rm E}_{j-1,k}, \qquad (3.44)
$$

$$
\Delta^x_{j,k} f := f(u^{\rm E}_{j,k}) - f(u^{\rm W}_{j,k}), \quad \Delta^x_{j+\frac12,k} f := f(u^{\rm W}_{j+1,k}) - f(u^{\rm E}_{j,k}), \quad \Delta^x_{j-\frac12,k} f := f(u^{\rm W}_{j,k}) - f(u^{\rm E}_{j-1,k}), \qquad (3.45)
$$

and a similar notation for the function g and the differences in the y-direction. The RHS of (3.43) can be rewritten as a linear combination of the point values of u along the boundaries of the (j,k)-cell,

$$
\begin{aligned}
u^{n+1}_{j,k} \;=\;& \lambda^n \left(\frac{a^-_{j+\frac12,k}}{(a^+_{j+\frac12,k} - a^-_{j+\frac12,k})} \frac{\Delta^x_{j+\frac12,k} f}{\Delta^x_{j+\frac12,k} u} - \frac{a^+_{j+\frac12,k} a^-_{j+\frac12,k}}{(a^+_{j+\frac12,k} - a^-_{j+\frac12,k})} \right) u^{\rm W}_{j+1,k} + \\
+\;& \lambda^n \left(\frac{a^+_{j-\frac12,k}}{(a^+_{j-\frac12,k} - a^-_{j-\frac12,k})} \frac{\Delta^x_{j-\frac12,k} f}{\Delta^x_{j-\frac12,k} u} - \frac{a^+_{j-\frac12,k} a^-_{j-\frac12,k}}{(a^+_{j-\frac12,k} - a^-_{j-\frac12,k})} \right) u^{\rm E}_{j-1,k} + \\
+\;& \left(\frac14 - \lambda^n \frac{a^-_{j+\frac12,k}}{(a^+_{j+\frac12,k} - a^-_{j+\frac12,k})} \frac{\Delta^x_{j+\frac12,k} f}{\Delta^x_{j+\frac12,k} u} - \lambda^n \frac{\Delta^x_{j,k} f}{\Delta^x_{j,k} u} + \lambda^n \frac{a^+_{j+\frac12,k} a^-_{j+\frac12,k}}{(a^+_{j+\frac12,k} - a^-_{j+\frac12,k})} \right) u^{\rm E}_{j,k} + \\
+\;& \left(\frac14 - \lambda^n \frac{a^+_{j-\frac12,k}}{(a^+_{j-\frac12,k} - a^-_{j-\frac12,k})} \frac{\Delta^x_{j-\frac12,k} f}{\Delta^x_{j-\frac12,k} u} + \lambda^n \frac{\Delta^x_{j,k} f}{\Delta^x_{j,k} u} + \lambda^n \frac{a^+_{j-\frac12,k} a^-_{j-\frac12,k}}{(a^+_{j-\frac12,k} - a^-_{j-\frac12,k})} \right) u^{\rm W}_{j,k} + \\
+\;& \mu^n \left(\frac{b^-_{j,k+\frac12}}{(b^+_{j,k+\frac12} - b^-_{j,k+\frac12})} \frac{\Delta^y_{j,k+\frac12} g}{\Delta^y_{j,k+\frac12} u} - \frac{b^+_{j,k+\frac12} b^-_{j,k+\frac12}}{(b^+_{j,k+\frac12} - b^-_{j,k+\frac12})} \right) u^{\rm S}_{j,k+1} + \\
+\;& \mu^n \left(\frac{b^+_{j,k-\frac12}}{(b^+_{j,k-\frac12} - b^-_{j,k-\frac12})} \frac{\Delta^y_{j,k-\frac12} g}{\Delta^y_{j,k-\frac12} u} - \frac{b^+_{j,k-\frac12} b^-_{j,k-\frac12}}{(b^+_{j,k-\frac12} - b^-_{j,k-\frac12})} \right) u^{\rm N}_{j,k-1} + \\
+\;& \left(\frac14 - \mu^n \frac{b^-_{j,k+\frac12}}{(b^+_{j,k+\frac12} - b^-_{j,k+\frac12})} \frac{\Delta^y_{j,k+\frac12} g}{\Delta^y_{j,k+\frac12} u} - \mu^n \frac{\Delta^y_{j,k} g}{\Delta^y_{j,k} u} + \mu^n \frac{b^+_{j,k+\frac12} b^-_{j,k+\frac12}}{(b^+_{j,k+\frac12} - b^-_{j,k+\frac12})} \right) u^{\rm N}_{j,k} + \\
+\;& \left(\frac14 - \mu^n \frac{b^+_{j,k-\frac12}}{(b^+_{j,k-\frac12} - b^-_{j,k-\frac12})} \frac{\Delta^y_{j,k-\frac12} g}{\Delta^y_{j,k-\frac12} u} + \mu^n \frac{\Delta^y_{j,k} g}{\Delta^y_{j,k} u} + \mu^n \frac{b^+_{j,k-\frac12} b^-_{j,k-\frac12}}{(b^+_{j,k-\frac12} - b^-_{j,k-\frac12})} \right) u^{\rm S}_{j,k}. \qquad (3.46)
\end{aligned}
$$

Here, the sum of all the coefficients is one, and due to our CFL assumption (3.42) and the definition of $a^\pm, b^\pm$, they are positive: for example, let us consider the last coefficient. Dropping all superscripts n and subscripts $j, k-\frac12$ we obtain:

$$
\begin{aligned}
& \frac14 - \mu \frac{b^+}{(b^+ - b^-)} \frac{\Delta^y g}{\Delta^y u} + \mu \frac{\Delta^y_{j,k} g}{\Delta^y_{j,k} u} + \mu \frac{b^+ b^-}{(b^+ - b^-)} \\
\geq\;& \frac18 + \mu \frac{b^+}{(b^+ - b^-)} \left(b^- - \frac{\Delta^y g}{\Delta^y u} \right)
\end{aligned}
$$

$$
\begin{aligned}
&\geq \frac{1}{8}+\mu\frac{b^+}{(b^+-b^-)}\left(b^- - b^+\right)\\
&= \frac{1}{8}-\mu b^+ \geq 0.
\end{aligned}
\tag{3.47}
$$

Hence, $u_{j,k}^{n+1}$ is a *convex* combination of $u^{\rm W}_{j+1,k}$, $u^{\rm E}_{j-1,k}$, $u^{\rm W}_{j,k}$, $u^{\rm E}_{j,k}$, $u^{\rm S}_{j,k+1}$, $u^{\rm N}_{j,k-1}$, $u^{\rm N}_{j,k}$, and $u^{\rm S}_{j,k}$. Further, the TVD property of the minmod limiter ensures that

$$
\begin{aligned}
\min_{j,k}\{u^n_{j,k}\} &\leq \min_{j,k}\{u^{\rm W}_{j+1,k},u^{\rm E}_{j-1,k},u^{\rm W}_{j,k},u^{\rm E}_{j,k},u^{\rm S}_{j,k+1},u^{\rm N}_{j,k-1},u^{\rm N}_{j,k},u^{\rm S}_{j,k}\}\leq\\
&\leq \max_{j,k}\{u^{\rm W}_{j+1,k},u^{\rm E}_{j-1,k},u^{\rm W}_{j,k},u^{\rm E}_{j,k},u^{\rm S}_{j,k+1},u^{\rm N}_{j,k-1},u^{\rm N}_{j,k},u^{\rm S}_{j,k}\} \leq \max_{j,k}\{u^n_{j,k}\},
\end{aligned}
$$

and the maximum principle (3.41) follows. ∎

Remark. The theorem still holds if instead of (2.9) we use the generalized minmod limiter

$$
s_j^n = \mathrm{minmod}\left(\theta\frac{\bar u_j^n-\bar u_{j-1}^n}{\Delta x},\frac{\bar u_{j+1}^n-\bar u_{j-1}^n}{2\Delta x},\theta\frac{\bar u_{j+1}^n-\bar u_j^n}{\Delta x}\right),\quad 1\leq\theta\leq 2.
$$

3.4 Semi-discrete central-upwind scheme for Hamilton-Jacobi equations

In this section, we propose a new Godunov-type central-upwind scheme for the one- and two-dimensional Hamilton-Jacobi equations (1.2). We follow the approach in [27], but this time we utilize a more precise information about the *one-sided* local speeds of propagation.

We begin with the one-dimensional case and start at time level $t=t^n$ with the continuous piecewise polynomial interpolant $\widetilde\varphi(x,t^n)$, and estimate the maximal one-sided local speeds, a_j^+ and a_j^-. For example, in the convex case, they are equal to

$$
a_j^+ := \max\{H'(\varphi_x^+),H'(\varphi_x^-),0\},\qquad a_j^- := \min\{H'(\varphi_x^+),H'(\varphi_x^-),0\},
\tag{3.48}
$$

where we use the notation $\varphi_x^\pm := \widetilde\varphi_x(x_j\pm 0,t^n)$. To construct the second-order scheme one should use the continuous piecewise quadratic polynomial (2.11), and in this case,

$$
\varphi_x^\pm = \frac{(\Delta\varphi)^n_{j\pm\frac12}}{\Delta x}\mp\frac{(\Delta\varphi)'_{j\pm\frac12}}{2\Delta x}.
\tag{3.49}
$$

Note that under an appropriate CFL-condition, the solution of the Hamilton-Jacobi equation (1.2) with the piecewise polynomial initial data $\widetilde\varphi(x,t^n)$ is smooth along the line segments $(x^n_{j\pm},t)$, $t^n\leq t<t^{n+1}$, $x^n_{j\pm}:=x_j+a_j^\pm\Delta t$, see Figure 3.3. Therefore, one can use the Taylor expansion to compute the intermediate point values at the next time level

$$
\varphi^{n+1}_{j\pm} = \widetilde\varphi(x_{j\pm},t^n)-\Delta t\cdot H(\widetilde\varphi_x(x^n_{j\pm},t^n))+\mathcal{O}(\Delta t)^2.
\tag{3.50}
$$

We complete the construction of our fully-discrete central-upwind scheme by projecting the intermediate point values back onto the original grid. Since the distance between x^n_{j+} and x^n_{j-} is proportional to Δt, it suffices to compute the weighted averages of φ^{n+1}_{j+} and φ^{n+1}_{j-}, that is

$$
\varphi_j^{n+1} = \frac{a_j^+}{a_j^+-a_j^-}\varphi^{n+1}_{j-}-\frac{a_j^-}{a_j^+-a_j^-}\varphi^{n+1}_{j+}+\mathcal{O}(\Delta t)^2.
\tag{3.51}
$$

Finally, we substitute (3.50) in (3.51), and arrive at the fully-discrete scheme

$$\begin{aligned}\varphi_j^{n+1} &= \frac{a_j^+}{a_j^+ - a_j^-}\Big(\widetilde{\varphi}(x_{j-},t^n) - \Delta t H(\widetilde{\varphi}_x(x_{j-}^n,t^n))\Big) - \\ &- \frac{a_j^-}{a_j^+ - a_j^-}\Big(\widetilde{\varphi}(x_{j+},t^n) - \Delta t H(\widetilde{\varphi}_x(x_{j+}^n,t^n))\Big) + \mathcal{O}(\Delta t)^2,\end{aligned} \tag{3.52}$$

which is high-order in space (depending on the order of the piecewise polynomial reconstruction), and only first-order in time.

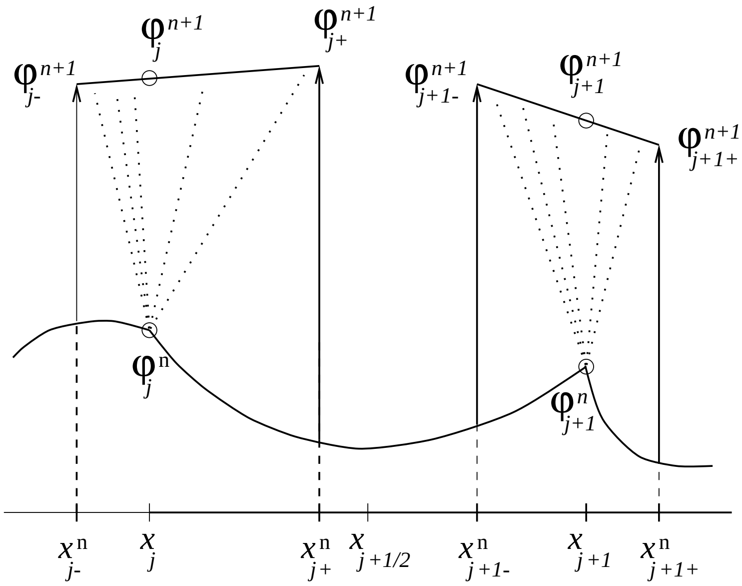

Figure 3.3: Central-upwind differencing – 1D.

A semi-discrete version of the scheme (3.52), coupled with a high-order ODE solver, will allow us to achieve high accuracy both in space and time. To derive such a scheme, we first use the Taylor expansions

$$\widetilde{\varphi}(x_{j\pm},t^n) = \widetilde{\varphi}(x_j,t^n) + \Delta t a_j^{\pm}\widetilde{\varphi}_x(x_j \pm 0,t^n) + \mathcal{O}(\Delta t)^2,$$

and rewrite the fully-discrete scheme (3.52) as

$$\begin{aligned}\varphi_j^{n+1} = \varphi_j^n \quad &- \quad \Delta t\frac{a_j^+ a_j^-}{a_j^+ - a_j^-}\Big[\widetilde{\varphi}_x(x_j+0,t^n) - \widetilde{\varphi}_x(x_j-0,t^n)\Big] + \\ &+ \quad \frac{\Delta t}{a_j^+ - a_j^-}\Big[a_j^- H(\widetilde{\varphi}_x(x_{j+}^n,t^n)) - a_j^+ H(\widetilde{\varphi}_x(x_{j-}^n,t^n))\Big] + \mathcal{O}(\Delta t)^2.\end{aligned} \tag{3.53}$$

We now let $\Delta t \to 0$, and end up with the following semi-discrete central-upwind scheme,

$$\frac{d}{dt}\varphi_j(t) = \frac{1}{a_j^+ - a_j^-}\Big[a_j^- H(\varphi_x^+) - a_j^+ H(\varphi_x^-)\Big] - \frac{a_j^+ a_j^-}{a_j^+ - a_j^-}\Big(\varphi_x^+ - \varphi_x^-\Big). \tag{3.54}$$

Here, $a_j^{\pm}$ are given by (3.48), and $\varphi_x^{\pm}$ are the right and the left derivatives at the point $x = x_j$ of the reconstruction $\widetilde{\varphi}(\cdot,t)$ at time t.

Remark. The spatial order of the scheme (3.54) is equal to the order of the piecewise polynomial reconstruction, $\widetilde{\varphi}$. For example, the second-order scheme, used in our numerical experiments, is based on the piecewise quadratic reconstruction (2.11).

We continue with the construction of a multidimensional extension of the scheme (3.54). Without loss of generality, we consider the two-dimensional Hamilton-Jacobi equation,

$$\varphi_t + H(\varphi_x, \varphi_y) = 0. \tag{3.55}$$

Assume that at time $t = t^n$ the discrete approximation to the point values of its solution, $\{\varphi^n_{j,k} \approx \varphi(x_j, y_k, t^n)\}$, has been already computed. We then construct the two-dimensional continuous piecewise polynomial interpolant $\widetilde{\varphi}(x, y, t^n)$. Such a reconstruction is defined over the four triangles (NW, NE, SW and SE) around each grid-point (x_j, y_k) (see Figure 3.4). For example, the second-order piecewise quadratic interpolant is

$$\begin{aligned}
\widetilde{\varphi}^{\mathrm{NE(NW)}}(x,y) \;=\;& \varphi^n_{j,k} + \frac{(\Delta\varphi)^n_{j\pm\frac12,k}}{\Delta x}(x-x_j) + \frac{(\Delta\varphi)^n_{j,k+\frac12}}{\Delta y}(y-y_k) + \frac{(\Delta\varphi)'_{j\pm\frac12,k}}{2(\Delta x)^2}(x-x_j)(x-x_{j\pm1}) \\
&+ \frac{(\Delta\varphi)^{\backprime}_{j,k+\frac12}}{2(\Delta y)^2}(y-y_k)(y-y_{k+1}) + \frac{(\Delta\varphi)'_{j,k+\frac12} + (\Delta\varphi)^{\backprime}_{j\pm\frac12,k}}{2\Delta x\Delta y}(x-x_j)(y-y_k), \qquad (3.56)\\
\widetilde{\varphi}^{\mathrm{SE(SW)}}(x,y) \;=\;& \varphi^n_{j,k} + \frac{(\Delta\varphi)^n_{j\pm\frac12,k}}{\Delta x}(x-x_j) + \frac{(\Delta\varphi)^n_{j,k-\frac12}}{\Delta y}(y-y_k) + \frac{(\Delta\varphi)'_{j\pm\frac12,k}}{2(\Delta x)^2}(x-x_j)(x-x_{j\pm1}) \\
&+ \frac{(\Delta\varphi)^{\backprime}_{j,k-\frac12}}{2(\Delta y)^2}(y-y_k)(y-y_{k-1}) + \frac{(\Delta\varphi)'_{j,k-\frac12} + (\Delta\varphi)^{\backprime}_{j\pm\frac12,k}}{2\Delta x\Delta y}(x-x_j)(y-y_k). \qquad (3.57)
\end{aligned}$$

Here, we use the notation $(\Delta\varphi)^n_{j+\frac12,k} := \varphi^n_{j+1,k} - \varphi^n_{j,k}$, $(\Delta\varphi)^n_{j,k+\frac12} := \varphi^n_{j,k+1} - \varphi^n_{j,k}$; and

$$\frac{(\Delta\varphi)'_{j+\frac12,k}}{(\Delta x)^2}, \quad \frac{(\Delta\varphi)'_{j,k+\frac12}}{\Delta x\Delta y}, \quad \frac{(\Delta\varphi)^{\backprime}_{j+\frac12,k}}{\Delta x\Delta y}, \quad \frac{(\Delta\varphi)^{\backprime}_{j,k+\frac12}}{(\Delta y)^2} \tag{3.58}$$

stand for the approximations to the corresponding exact derivatives

$$\varphi_{xx}(x_{j+\frac12}, y_k, t^n), \quad \varphi_{xy}(x_j, y_{k+\frac12}, t^n), \quad \varphi_{xy}(x_{j+\frac12}, y_k, t^n), \quad \varphi_{yy}(x_j, y_{k+\frac12}, t^n).$$

The numerical derivatives (3.58) can be computed, for example, by using the minmod limiter (2.13), applied in an appropriate direction, namely

$$\begin{aligned}
(\Delta\varphi)^{\backprime}_{j+\frac12,k} =\ & \mathrm{minmod}\left(\theta\left[(\Delta\varphi)^n_{j+\frac12,k+1} - (\Delta\varphi)^n_{j+\frac12,k}\right], \frac12\left[(\Delta\varphi)^n_{j+\frac12,k+1} - (\Delta\varphi)^n_{j+\frac12,k-1}\right],\right.\\
&\qquad\qquad \left.\theta\left[(\Delta\varphi)^n_{j+\frac12,k} - (\Delta\varphi)^n_{j+\frac12,k-1}\right]\right),\\
(\Delta\varphi)^{\backprime}_{j,k+\frac12} =\ & \mathrm{minmod}\left(\theta\left[(\Delta\varphi)^n_{j,k+\frac32} - (\Delta\varphi)^n_{j,k+\frac12}\right], \frac12\left[(\Delta\varphi)^n_{j,k+\frac32} - (\Delta\varphi)^n_{j,k-\frac12}\right],\right.\\
&\qquad\qquad \left.\theta\left[(\Delta\varphi)^n_{j,k+\frac12} - (\Delta\varphi)^n_{j,k-\frac12}\right]\right).
\end{aligned}$$

Other numerical derivatives in (3.58) can be approximated in a similar manner.

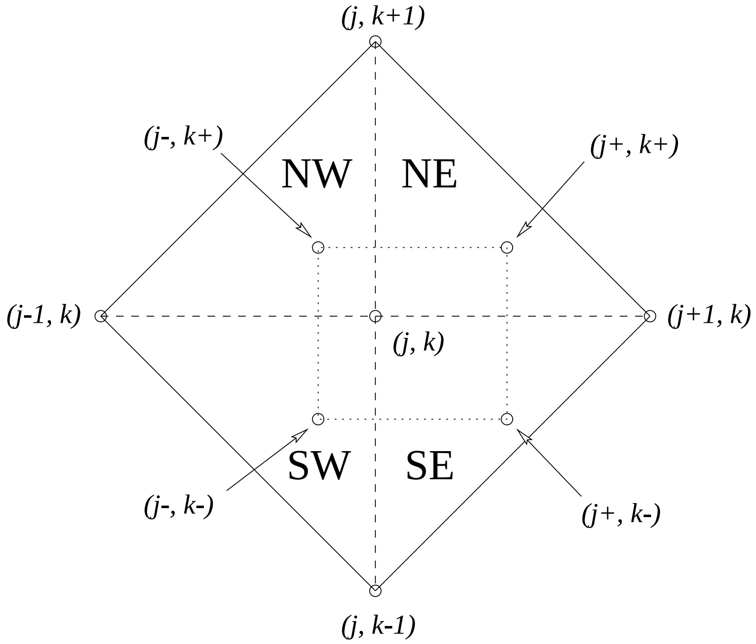

Figure 3.4: Central-upwind differencing – 2D.

We now continue with the construction of our semi-discrete central-upwind scheme. As in the one-dimensional case, we use the maximal values of the one-sided local speeds of propagation in the x- and y-directions. These values at the grid-point (x_j, y_k) are given by

$$\begin{aligned} a^+_{j,k} &:= \max_{C_{j,k}} \Big\{ H_u(\widetilde{\varphi}_x(x,y), \widetilde{\varphi}_y(x,y)) \Big\}_+, \quad a^-_{j,k} := \min_{C_{j,k}} \Big\{ H_u(\widetilde{\varphi}_x(x,y), \widetilde{\varphi}_y(x,y)) \Big\}_-, \\ b^+_{j,k} &:= \max_{C_{j,k}} \Big\{ H_v(\widetilde{\varphi}_x(x,y), \widetilde{\varphi}_y(x,y)) \Big\}_+, \quad b^-_{j,k} := \min_{C_{j,k}} \Big\{ H_v(\widetilde{\varphi}_x(x,y), \widetilde{\varphi}_y(x,y)) \Big\}_-, \end{aligned} \tag{3.59}$$

where $C_{j,k} := [x_{j-\frac{1}{2}}, x_{j+\frac{1}{2}}] \times [y_{k-\frac{1}{2}}, y_{k+\frac{1}{2}}]$, and $(\cdot)_+ := \max(\cdot, 0)$, $(\cdot)_- := \min(\cdot, 0)$.

To compute the solution at the next time level $t = t^{n+1}$, we use the intermediate values $\{\varphi^{n+1}_{j\pm,k\pm}\}$, obtained by the Taylor expansion about the points $(x^n_{j\pm} := x_j + a^\pm_{j,k}\Delta t,\ y^n_{k\pm} := y_k + b^\pm_{j,k}\Delta t)$,

$$\varphi^{n+1}_{j\pm,k\pm} = \widetilde{\varphi}(x^n_{j\pm}, y^n_{k\pm}, t^n) - \Delta t \cdot H(\widetilde{\varphi}_x(x^n_{j\pm}, y^n_{k\pm}, t^n), \widetilde{\varphi}_y(x^n_{j\pm}, y^n_{k\pm}, t^n)) + \mathcal{O}(\Delta t)^2. \tag{3.60}$$

Expansion (3.60) is valid, since due to the finite speed of propagation, the solution of (3.55) with the initial data $\widetilde{\varphi}(x, y, t^n)$ is smooth around $(x^n_{j\pm}, y^n_{k\pm})$, see Figure 3.4.

Next, the computed intermediate values (3.60) are projected back onto the original grid. This can be done using the weighted average of the values $\varphi^{n+1}_{j\pm,k\pm}$, since the distance between the points $(x_{j\pm}, y_{k\pm})$ is proportional to $\mathcal{O}(\Delta t)$. The resulting fully-discrete scheme is

$$\begin{aligned} \varphi^{n+1}_{j,k} &= \frac{a^-_{j,k} b^-_{j,k} \varphi^{n+1}_{j+,k+} - a^-_{j,k} b^+_{j,k} \varphi^{n+1}_{j+,k-} - a^+_{j,k} b^-_{j,k} \varphi^{n+1}_{j-,k+} + a^+_{j,k} b^+_{j,k} \varphi^{n+1}_{j-,k-}}{(a^+_{j,k} - a^-_{j,k})(b^+_{j,k} - b^-_{j,k})} + \mathcal{O}(\Delta t)^2 = \\ &= \frac{a^-_{j,k} b^-_{j,k}}{(a^+_{j,k} - a^-_{j,k})(b^+_{j,k} - b^-_{j,k})} \Big(\widetilde{\varphi}(x^n_{j+}, y^n_{k+}, t^n) - \Delta t \cdot H(\widetilde{\varphi}_x(x^n_{j+}, y^n_{k+}, t^n), \widetilde{\varphi}_y(x^n_{j+}, y^n_{k+}, t^n)) \Big) - \\ &- \frac{a^-_{j,k} b^+_{j,k}}{(a^+_{j,k} - a^-_{j,k})(b^+_{j,k} - b^-_{j,k})} \Big(\widetilde{\varphi}(x^n_{j+}, y^n_{k-}, t^n) - \Delta t \cdot H(\widetilde{\varphi}_x(x^n_{j+}, y^n_{k-}, t^n), \widetilde{\varphi}_y(x^n_{j+}, y^n_{k-}, t^n)) \Big) - \end{aligned}$$

$$
\begin{aligned}
&- \frac{a^+_{j,k}b^-_{j,k}}{(a^+_{j,k}-a^-_{j,k})(b^+_{j,k}-b^-_{j,k})}\Big(\widetilde{\varphi}(x^n_{j-},y^n_{k+},t^n) - \Delta t\cdot H(\widetilde{\varphi}_x(x^n_{j-},y^n_{k+},t^n),\widetilde{\varphi}_y(x^n_{j-},y^n_{k+},t^n))\Big) + \\
&+ \frac{a^+_{j,k}b^+_{j,k}}{(a^+_{j,k}-a^-_{j,k})(b^+_{j,k}-b^-_{j,k})}\Big(\widetilde{\varphi}(x^n_{j-},y^n_{k-},t^n) - \Delta t\cdot H(\widetilde{\varphi}_x(x^n_{j-},y^n_{k-},t^n),\widetilde{\varphi}_y(x^n_{j-},y^n_{k-},t^n))\Big) + \\
&\quad +\mathcal{O}(\Delta t)^2.
\end{aligned}
\tag{3.61}
$$

As in the one-dimensional case, the fully-discrete central-upwind scheme (3.61) is only first-order in time. This disadvantage can be eliminated by passing to the semi-discrete limit in (3.61) as $\Delta t \to 0$. To this end, we first compute the values of $\widetilde{\varphi}(x^n_{\pm}, y^n_{\pm}, t^n)$ by the Taylor expansions

$$
\begin{aligned}
\widetilde{\varphi}(x_{j\pm},y_{k+},t^n) &= \widetilde{\varphi}(x_j,y_k,t^n) + \Delta t a^{\pm}_{j,k}\widetilde{\varphi}_x(x_j\pm 0,y_k,t^n) + \Delta t b^+_{j,k}\widetilde{\varphi}_y(x_j,y_k+0,t^n) + \mathcal{O}(\Delta t)^2,\\
\widetilde{\varphi}(x_{j\pm},y_{k-},t^n) &= \widetilde{\varphi}(x_j,y_k,t^n) + \Delta t a^{\pm}_{j,k}\widetilde{\varphi}_x(x_j\pm 0,y_k,t^n) + \Delta t b^-_{j,k}\widetilde{\varphi}_y(x_j,y_k-0,t^n) + \mathcal{O}(\Delta t)^2.
\end{aligned}
$$

We then plug these values in (3.61), obtaining

$$
\begin{aligned}
\varphi^{n+1}_{j,k} = \varphi^n_{j,k} \;&-\; \Delta t\frac{a^+_{j,k}a^-_{j,k}}{a^+_{j,k}-a^-_{j,k}}\Big[\widetilde{\varphi}_x(x_j+0,y_k,t^n) - \widetilde{\varphi}_x(x_j-0,y_k,t^n)\Big] - \\
&-\; \Delta t\frac{b^+_{j,k}b^-_{j,k}}{b^+_{j,k}-b^-_{j,k}}\Big[\widetilde{\varphi}_y(x_j,y_k+0,t^n) - \widetilde{\varphi}_y(x_j,y_k-0,t^n)\Big] - \\
&-\; \frac{\Delta t}{(a^+_{j,k}-a^-_{j,k})(b^+_{j,k}-b^-_{j,k})}\Big[a^-_{j,k}b^-_{j,k}H(\widetilde{\varphi}_x(x^n_{j+},y^n_{k+},t^n)) - a^-_{j,k}b^+_{j,k}H(\widetilde{\varphi}_x(x^n_{j+},y^n_{k-},t^n)) - \\
&\qquad -a^+_{j,k}b^-_{j,k}H(\widetilde{\varphi}_x(x^n_{j-},y^n_{k+},t^n)) + a^+_{j,k}b^+_{j,k}H(\widetilde{\varphi}_x(x^n_{j-},y^n_{k-},t^n))\Big].
\end{aligned}
\tag{3.62}
$$

Finally, we subtract $\varphi^n_{j,k}$ from the both sides of (3.62), divide by Δt and pass to the limit as $\Delta t \to 0$. This results in the *two-dimensional semi-discrete central-upwind scheme*

$$
\begin{aligned}
\frac{d}{dt}\varphi_{j,k}(t) \;=\; &-\frac{a^-_{j,k}b^-_{j,k}H(\varphi^+_x,\varphi^+_y) - a^-_{j,k}b^+_{j,k}H(\varphi^+_x,\varphi^-_y) - a^+_{j,k}b^-_{j,k}H(\varphi^-_x,\varphi^+_y) + a^+_{j,k}b^+_{j,k}H(\varphi^-_x,\varphi^-_y)}{(a^+_{j,k}-a^-_{j,k})(b^+_{j,k}-b^-_{j,k})} - \\
&-\frac{a^+_{j,k}a^-_{j,k}}{a^+_{j,k}-a^-_{j,k}}\Big(\varphi^+_x-\varphi^-_x\Big) - \frac{b^+_{j,k}b^-_{j,k}}{b^+_{j,k}-b^-_{j,k}}\Big(\varphi^+_y-\varphi^-_y\Big).
\end{aligned}
\tag{3.63}
$$

Here, $\varphi^{\pm}_x := \widetilde{\varphi}_x(x_j \pm 0, y_k, t)$ and $\varphi^{\pm}_y := \widetilde{\varphi}_y(x_j, y_k \pm 0, t)$ are the right and the left derivatives in the x- and y-direction, respectively. For example, for the second-order reconstruction (3.56)–(3.57), these derivatives are

$$
\varphi^{\pm}_x = \frac{(\Delta\varphi)^n_{j\pm\frac12,k}}{\Delta x} \mp \frac{(\Delta\varphi)'_{j\pm\frac12,k}}{2\Delta x}, \qquad \varphi^{\pm}_y = \frac{(\Delta\varphi)^n_{j,k\pm\frac12}}{\Delta y} \mp \frac{(\Delta\varphi)^{\backslash}_{j,k\pm\frac12}}{2\Delta y}.
\tag{3.64}
$$

The one-sided local speeds in (3.63) are given by (3.59). In practice, these speeds can be estimated in a simpler way. For instance, in the numerical examples, we have used

$$
\begin{aligned}
a^+_{j,k} &:= \max_{\pm}\Big\{H_u(\varphi^{\pm}_x,\varphi^{\pm}_y)\Big\}_+, \qquad a^-_{j,k} := \min_{\pm}\Big\{H_u(\varphi^{\pm}_x,\varphi^{\pm}_y)\Big\}_-,\\
b^+_{j,k} &:= \max_{\pm}\Big\{H_v(\varphi^{\pm}_x,\varphi^{\pm}_y)\Big\}_+, \qquad b^-_{j,k} := \min_{\pm}\Big\{H_v(\varphi^{\pm}_x,\varphi^{\pm}_y)\Big\}_-.
\end{aligned}
\tag{3.65}
$$

Finally, to obtain the same second-order accuracy in time, our semi-discrete central-upwind scheme (3.63)–(3.65) should be complemented with at least second-order ODE solver for time discretization.

4 Numerical examples

In this section, we implement our scheme for conservation laws and Hamilton-Jacobi equations, and perform several numerical experiments. We test the accuracy of the scheme on problems with smooth solutions, and solve various equations which admit nonsmooth solutions. Among them are the Euler equations of gas dynamics, the incompressible Euler equations, and others. The numerical results show that our scheme gives sharper resolution and reduces some of the side effects of the schemes from [27, 25].

The high-order semi-discrete methods, presented in this paper, require a time discretization of the corresponding order. In the numerical examples, shown below, we have used the third-order TVD Runge-Kutta method, proposed in [45, 47], and the second-order modified Euler method. Our choice is based on the stability properties of these methods, each time step of which can be viewed as a convex combination of small forward Euler steps.

In all the numerical experiments below, the CFL number is equal to 0.475, and the value of θ in the generalized minmod limiter is 2.

4.1 One-dimensional problems

Example 1 – Burgers' equation.

First, we consider the initial boundary value problem (IBVP) for the inviscid Burgers' equation

$$\begin{cases} u_t + \left(\dfrac{u^2}{2}\right)_x = 0, \quad x \in [0, 2\pi], \\ \\ u(x,0) = 0.5 + \sin x, \end{cases} \tag{4.1}$$

with periodic boundary conditions. It is known that the unique entropy solution of (4.1) develops a shock discontinuity at time $t = 1$. The solution at the pre-shock time $T = 0.5$ is smooth, and this allows us to test the accuracy of the one-dimensional third-order central-upwind scheme (3.13)–(3.15). We couple it with the basic piecewise quadratic reconstruction (2.5) and compute the solution using N grid points, $N = 40, 80, \dots, 1280$.

The L^∞- and L^1-errors are shown in Table 4.1. To calculate the errors, we use the computed values $\{\bar{u}_j\}$ at the final time, and the sliding averages $\{\bar{u}(x_j, T)\}$ of the exact solution of (4.1), namely

$$\|\bar{u} - \bar{u}(\cdot,T)\|_{L^\infty} := \max_j |\bar{u}_j - \bar{u}(x_j,T)|, \qquad \|\bar{u} - \bar{u}(\cdot,T)\|_{L^1} := \Delta x \sum_j |\bar{u}_j - \bar{u}(x_j,T)|.$$

These results clearly demonstrate a third-order experimental convergence rate.

Example 2 – One-dimensional Euler equations of gas dynamics.

We solve the one-dimensional Euler system,

$$\frac{\partial}{\partial t}\begin{bmatrix} \rho \\ m \\ E \end{bmatrix} + \frac{\partial}{\partial x}\begin{bmatrix} m \\ \rho u^2 + p \\ u(E+p) \end{bmatrix} = 0, \qquad p = (\gamma - 1)\cdot\left(E - \frac{\rho}{2}u^2\right), \tag{4.2}$$

with the initial data

$$\vec{u}(x,0) = \begin{cases} \vec{u}_L = (1, 0, 2500)^T, & 0 \le x < 0.1, \\ \vec{u}_M = (1, 0, 0.025)^T, & 0.1 \le x < 0.9, \\ \vec{u}_R = (1, 0, 250)^T, & 0.9 \le x < 1, \end{cases} \tag{4.3}$$

N	L^∞-error	rate	L^1-error	rate
40	1.456e-03	–	1.241e-03	–
80	2.177e-04	2.74	1.683e-04	2.88
160	2.893e-05	2.91	2.187e-05	2.94
320	3.689e-06	2.97	2.794e-06	2.97
640	4.559e-07	3.02	3.484e-07	3.00
1280	5.720e-08	2.99	4.376e-08	2.99

Table 4.1: Accuracy test for the Burgers' equation (4.1), **T=0.5**.

and solid wall boundary conditions, applied to both ends. This problem was proposed by Woodward and Colella in [51], and it models the interaction of blast waves. Here the value of $\gamma = 1.4$, and ρ, u, $m = \rho u$, p and E are the density, velocity, momentum, pressure and the total energy, respectively.

The solution is computed with our scheme (3.14)–(3.15) and the reconstruction (2.10). We use $N = 400$ grid points, and plot the density, the velocity and the pressure together with a reference solution, obtained by the same method with $N = 1600$.

Figures 4.1, 4.2, and 4.3 show the density, the velocity, and the pressure at time $T = .01$. Note, that for $N = 400$, the second density spike has a height of ~ 5.9, which is closer to the actual value of the solution. This result is better than the heights of ~ 5.75, ~ 5.2, and ~ 3.7, obtained by the third-order central schemes in [25], [39], and the second-order Nessyahu-Tadmor scheme in [40], respectively. This illustrates the higher resolution and smaller numerical dissipation of the central-upwind scheme.

The computations at times $T = 0.03$ and $T = 0.038$ are comparable to the results from [25], and are shown in Figures 4.4–4.6.

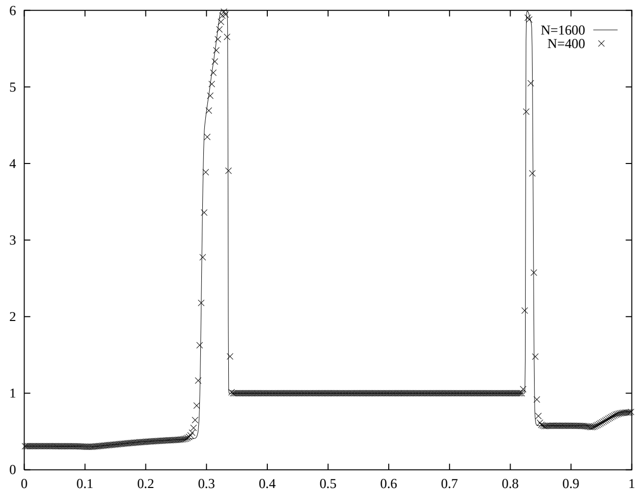

Figure 4.1: Problem (4.2)–(4.3), density at **T=0.01**.

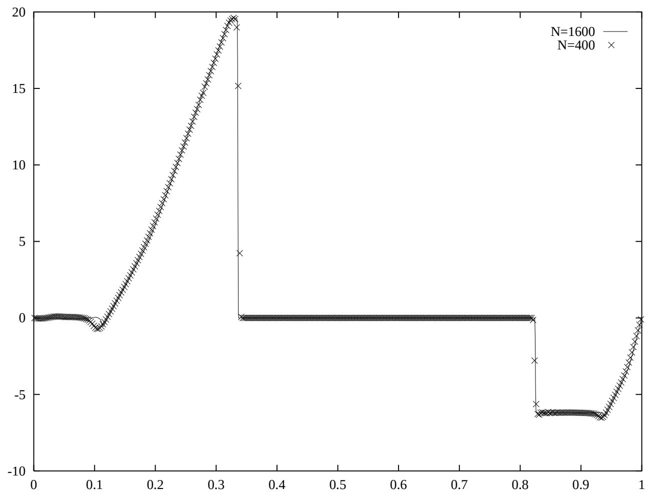

Figure 4.2: Problem (4.2)–(4.3), velocity at **T=0.01**.

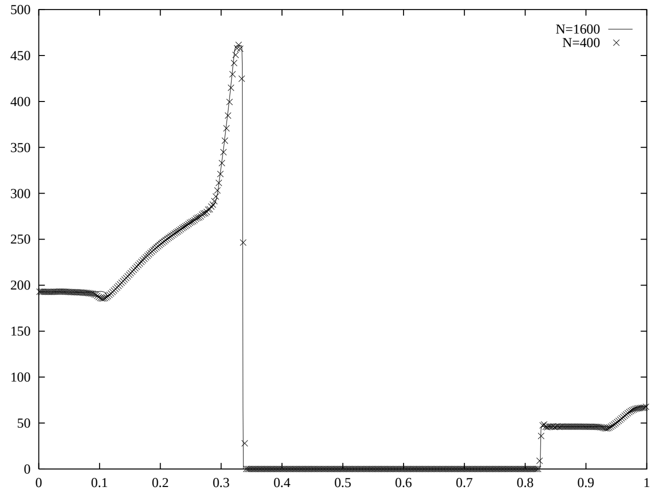

Figure 4.3: Problem (4.2)–(4.3), pressure at **T=0.01**.

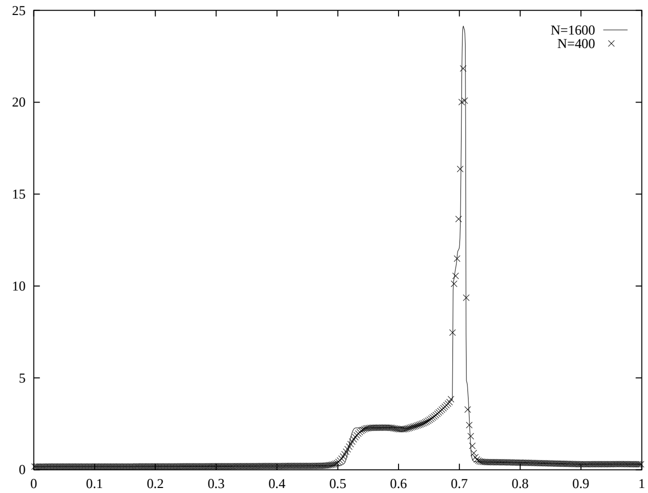

Figure 4.4: Problem (4.2)–(4.3), density at **T=0.03**.

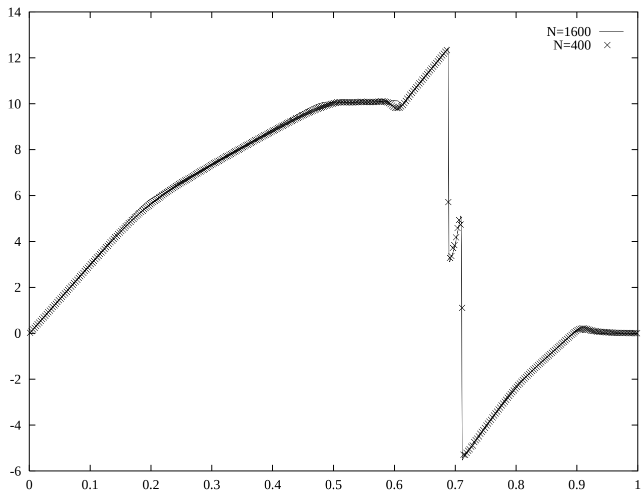

Figure 4.5: Problem (4.2)–(4.3), velocity at **T=0.03**.

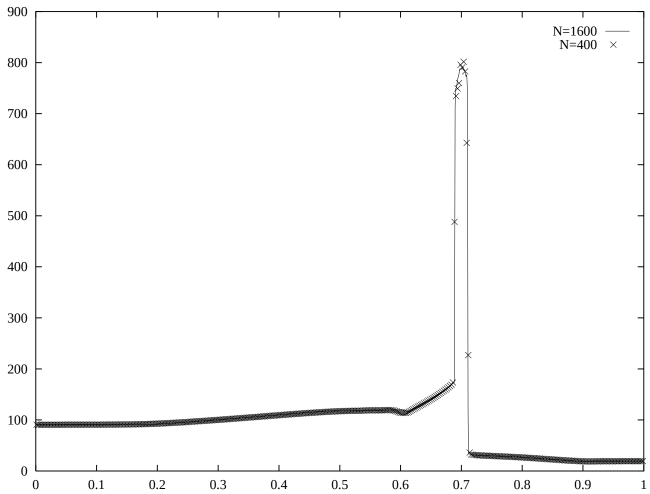

Figure 4.6: Problem (4.2)–(4.3), pressure at **T=0.03**.

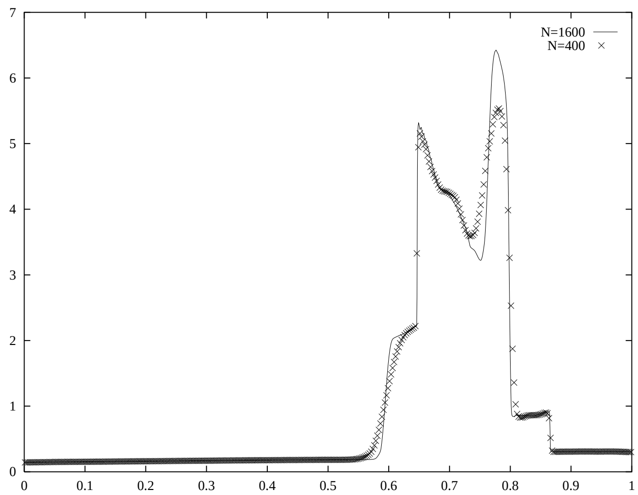

Figure 4.7: Problem (4.2)–(4.3), density at **T=0.038**.

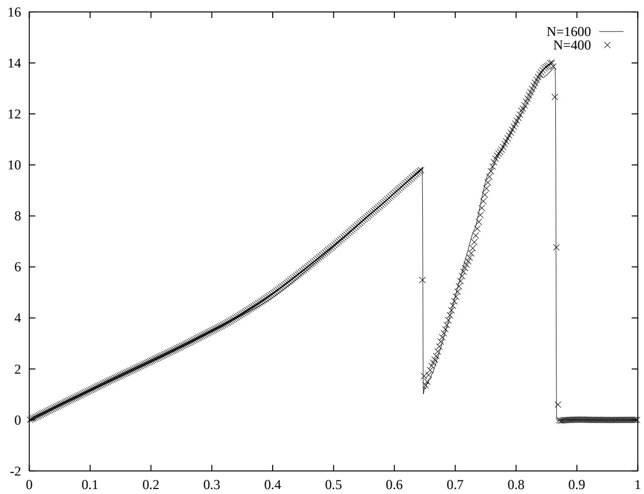

Figure 4.8: Problem (4.2)–(4.3), velocity at **T=0.038**.

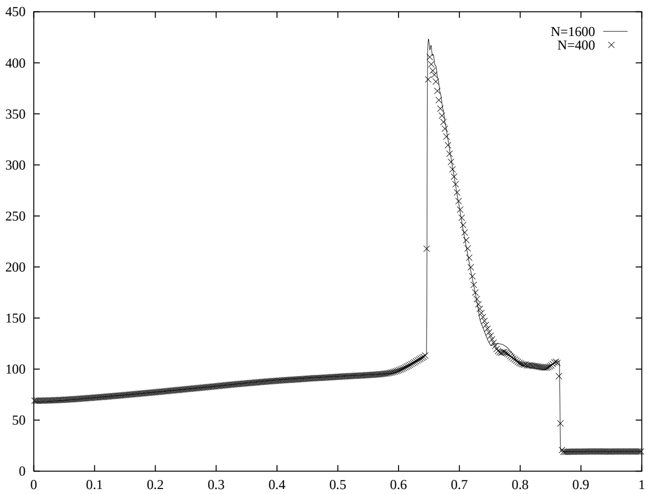

Figure 4.9: Problem (4.2)–(4.3), pressure at **T=0.038**.

Example 3 – One-dimensional Hamilton-Jacobi equation.

In this example, we apply the second-order central-upwind scheme (2.13),(3.48)–(3.49),(3.54) to the Riemann problem for a one-dimensional Hamilton-Jacobi equation with a non-convex Hamiltonian,

$$\begin{cases} \varphi_t + \frac{1}{4}(\varphi_x^2 - 1)(\varphi_x^2 - 4) = 0, \\ \varphi(x,0) = -2|x|. \end{cases} \tag{4.4}$$

The numerical solution, computed for different numbers of grid points is plotted in Figure 4.10. One can observe a very fast convergence of the approximate solutions towards the exact (viscosity) solution of (4.4) as the mesh is refined.

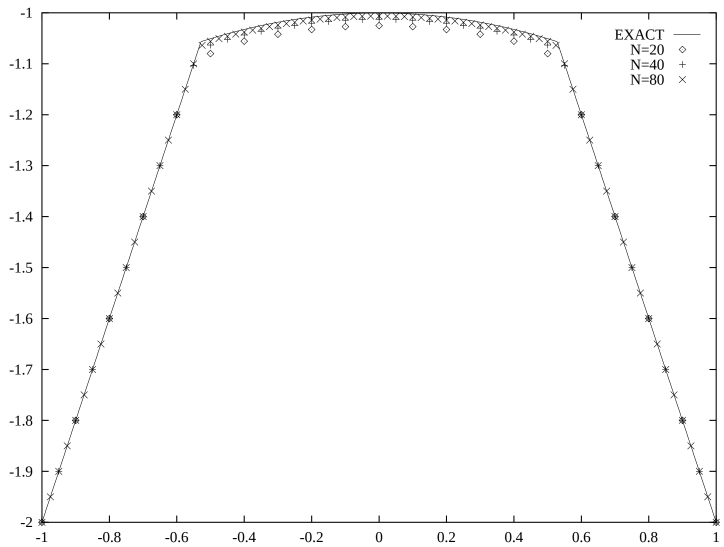

Figure 4.10: Problem (4.4), solution at **T=1**.

4.2 An example of a two-dimensional, third-order, piecewise quadratic reconstruction

In this section, we describe a third-order piecewise quadratic reconstruction, used in the next numerical examples. It was proposed in [25], and may be viewed as a generalization of the one-dimensional reconstruction (2.10). The main idea is to use a convex combination of the (possibly) oscillatory basic parabolas and non-oscillatory linear functions in order to construct a third-order non-oscillatory interpolant.

The resulting piecewise quadratic reconstruction $\{p^n_{j,k}\}$ is

$$p^n_{j,k}(x,y) = (1-\theta^n_{j,k})L^n_{j,k}(x,y) + \theta^n_{j,k}q^n_{j,k}(x,y), \qquad 0 < \theta^n_{j,k} < 1. \tag{4.5}$$

Here, $\{q^n_{j,k}\}$ is the basic parabola

$$\begin{aligned} q^n_{j,k}(x,y) \;\; = \;\; & \Big(\bar u^n_{j,k} - \frac{(\Delta x)^2}{24}D^x_+D^x_-\bar u^n_{j,k} - \frac{(\Delta y)^2}{24}D^y_+D^y_-\bar u^n_{j,k}\Big) + D^x_0\bar u^n_{j,k}(x-x_j) + D^y_0\bar u^n_{j,k}(y-y_k) + \\ & + \frac{1}{2}D^x_+D^x_-\bar u^n_{j,k}(x-x_j)^2 + D^x_0D^y_0\bar u^n_{j,k}(x-x_j)(y-y_k) + \frac{1}{2}D^y_+D^y_-\bar u^n_{j,k}(y-y_k)^2, \end{aligned} \tag{4.6}$$

where we use the notation

$$D^x_\pm v(x,y) := \pm\frac{v(x\pm\Delta x,y)-v(x,y)}{\Delta x}, \qquad D^y_\pm v(x,y) := \pm\frac{v(x,y\pm\Delta y)-v(x,y)}{\Delta y},$$

$$D^x_0 v(x,y) := \frac{v(x+\Delta x,y)-v(x-\Delta x,y)}{2\Delta x}, \qquad D^y_0 v(x,y) := \frac{v(x,y+\Delta y)-v(x,y-\Delta y)}{2\Delta y}.$$

The linear functions $\{L^n_{j,k}\}$ are given by

$$L^n_{j,k}(x,y) = \bar u^n_{j,k} + s^x_{j,k}(x-x_j) + s^y_{j,k}(y-y_k), \tag{4.7}$$

where the slopes $\{s^x_{j,k}, s^y_{j,k}\}$ are computed using the minmod limiter,

$$s^x_{j,k} = \text{minmod}\left(\frac{\bar u^n_{j,k}-\bar u^n_{j-1,k}}{\Delta x}, \frac{\bar u^n_{j+1,k}-\bar u^n_{j,k}}{\Delta x}\right), \quad s^y_{j,k} = \text{minmod}\left(\frac{\bar u^n_{j,k}-\bar u^n_{j,k-1}}{\Delta y}, \frac{\bar u^n_{j,k+1}-\bar u^n_{j,k}}{\Delta y}\right). \tag{4.8}$$

For our new scheme, only the eight point values $u^{\rm N}_{j,k}$, $u^{\rm E}_{j,k}$, $u^{\rm S}_{j,k}$, $u^{\rm W}_{j,k}$,$u^{\rm NE}_{j,k}$, $u^{\rm NW}_{j,k}$, $u^{\rm SE}_{j,k}$, and $u^{\rm SW}_{j,k}$ have to be computed in each (j,k)-cell. They may be calculated using the 'dimension-by-dimension' approach, applied in two steps.

First, we use the reconstruction (4.6)–(4.5) with

$$\theta^n_{j,k} = \min\{\theta^x_{j,k}, \theta^y_{j,k}\}, \tag{4.9}$$

to approximate the point values in the coordinate directions – $u^{\rm N}_{j,k}$, $u^{\rm E}_{j,k}$, $u^{\rm S}_{j,k}$ and $u^{\rm W}_{j,k}$. Here, the limiters $\{\theta^x_{j,k}\}$ and $\{\theta^y_{j,k}\}$ are determined by (2.8) with

$$L^n_j(\cdot) = L^n_{j,k}(\cdot, y_k), \qquad q_j(\cdot) = q^n_{j,k}(\cdot, y_k),$$

and

$$L^n_j(\cdot) = L^n_{j,k}(x_k, \cdot), \qquad q^n_j(\cdot) = L^n_{j,k}(x_k, \cdot).$$

To ensure that there are no oscillations in the diagonal directions, the point values $u^{\rm NE}_{j,k}$, $u^{\rm NW}_{j,k}$, $u^{\rm SE}_{j,k}$ and $u^{\rm SW}_{j,k}$ are computed by another reconstruction, which is determined by

$$\hat p^n_{j,k}(x,y) = (1-\hat\theta^n_{j,k})\hat L^n_{j,k}(x,y) + \hat\theta^n_{j,k}\hat q^n_{j,k}(x,y), \qquad 0 < \hat\theta^n_{j,k} < 1. \tag{4.10}$$

The adjusted basic parabolas $\{\hat q^n_{j,k}\}$ are

$$\begin{aligned}\hat q^n_{j,k}(x,y) = \Big(\bar u^n_{j,k} - \frac{\Delta^2}{48} D^{d^+}_+ D^{d^+}_- \bar u^n_{j,k} - \frac{\Delta^2}{48} D^{d^-}_+ D^{d^-}_- \bar u^n_{j,k}\Big) + D^{d^+}_0 \bar u^n_{j,k}\Big[\frac{\Delta}{2\Delta y}(y-y_k) + \frac{\Delta}{2\Delta x}(x-x_j)\Big] + \\ + D^{d^-}_0 \bar u^n_{j,k}\Big[\frac{\Delta}{2\Delta y}(y-y_k) - \frac{\Delta}{2\Delta x}(x-x_j)\Big] + D^{d^+}_0 D^{d^-}_0 \bar u^n_{j,k}\Big[\frac{\Delta^2}{4(\Delta y)^2}(y-y_k)^2 - \frac{\Delta^2}{4(\Delta x)^2}(x-x_j)^2\Big] + \\ + \frac{1}{2} D^{d^+}_+ D^{d^+}_- \bar u^n_{j,k}\Big[\frac{\Delta}{2\Delta y}(y-y_k) + \frac{\Delta}{2\Delta x}(x-x_j)\Big]^2 + \frac{1}{2} D^{d^-}_+ D^{d^-}_- \bar u^n_{j,k}\Big[\frac{\Delta}{2\Delta y}(y-y_k) - \frac{\Delta}{2\Delta x}(x-x_j)\Big]^2\end{aligned} \tag{4.11}$$

where $\Delta := \sqrt{(\Delta x)^2 + (\Delta y)^2}$, and the divided differences in the diagonal directions are

$$D^{d^+}_\pm v(x,y) := \pm\frac{v(x\pm\Delta x, y\pm\Delta y) - v(x,y)}{\Delta}, \quad D^{d^+}_0 v(x,y) := \frac{v(x+\Delta x, y+\Delta y) - v(x-\Delta x, y-\Delta y)}{2\Delta},$$

$$D^{d^-}_\pm v(x,y) := \pm\frac{v(x\mp\Delta x, y\pm\Delta y) - v(x,y)}{\Delta}, \quad D^{d^-}_0 v(x,y) := \frac{v(x-\Delta x, y+\Delta y) - v(x+\Delta x, y-\Delta y)}{2\Delta}.$$

The corresponding linear functions $\{\hat L^n_{j,k}\}$ are given by

$$\hat L^n_{j,k}(x,y) = \bar u^n_{j,k} + \hat s^+_{j,k}\Big[\frac{\Delta}{2\Delta y}(y-y_k) + \frac{\Delta}{2\Delta x}(x-x_j)\Big] + \hat s^-_{j,k}\Big[\frac{\Delta}{2\Delta y}(y-y_k) - \frac{\Delta}{2\Delta x}(x-x_j)\Big], \tag{4.12}$$

where the slopes are computed using the minmod limiter, applied in the diagonal directions, that is,

$$\hat s^+_{j,k} = \operatorname{minmod}\left(\frac{\bar u^n_{j,k} - \bar u^n_{j-1,k-1}}{\Delta}, \frac{\bar u^n_{j+1,k+1} - \bar u^n_{j,k}}{\Delta}\right), \tag{4.13}$$

$$\hat s^-_{j,k} = \operatorname{minmod}\left(\frac{\bar u^n_{j,k} - \bar u^n_{j+1,k-1}}{\Delta}, \frac{\bar u^n_{j-1,k+1} - \bar u^n_{j,k}}{\Delta}\right). \tag{4.14}$$

The parameter $\hat\theta^n_{j,k}$ in (4.10) is determined by

$$\hat\theta^n_{j,k} = \min\{\hat\theta^+_{j,k}, \hat\theta^-_{j,k}\}, \tag{4.15}$$

where $\hat\theta^{+}_{j,k}$ and $\hat\theta^{-}_{j,k}$ are computed similarly to (2.8), namely

$$\theta^{\pm}_{j,k} := \begin{cases} \min\left\{\dfrac{M^{\pm}_{j\pm\frac12,k+\frac12}-\hat L^n_{j,k}(x_{j\pm\frac12},y_{k+\frac12})}{M^{\pm}_{j,k}-\hat L^n_{j,k}(x_{j\pm\frac12},y_{k+\frac12})},\dfrac{m^{\pm}_{j\mp\frac12,k-\frac12}-\hat L^n_{j,k}(x_{j\mp\frac12},y_{k-\frac12})}{m^{\pm}_{j,k}-\hat L^n_{j,k}(x_{j\mp\frac12},y_{k-\frac12})},1\right\}, & \\ \qquad\qquad\qquad\qquad\qquad\qquad \text{if} \quad \bar u^n_{j\mp1,k-1}<\bar u^n_{j,k}<\bar u^n_{j\pm1,k+1}, & \\ \min\left\{\dfrac{M^{\pm}_{j\mp\frac12,k-\frac12}-\hat L^n_{j,k}(x_{j\mp\frac12},y_{k-\frac12})}{M^{\pm}_{j,k}-\hat L^n_{j,k}(x_{j\mp\frac12},y_{k-\frac12})},\dfrac{m^{\pm}_{j\pm\frac12,k+\frac12}-\hat L^n_{j,k}(x_{j\pm\frac12},y_{k+\frac12})}{m^{\pm}_{j,k}-\hat L^n_{j,k}(x_{j\pm\frac12},y_{k+\frac12})},1\right\}, & \\ \qquad\qquad\qquad\qquad\qquad\qquad \text{if} \quad \bar u^n_{j\mp1,k-1}>\bar u^n_{j,k}>\bar u^n_{j\pm1,k+1}, & \\ 1, & \text{otherwise}, \end{cases} \tag{4.16}$$

where

$$M^{\pm}_{j,k}=\max\left\{\hat q^n_{j,k}(x_{j\pm\frac12},y_{k+\frac12}),\hat q^n_{j,k}(x_{j\mp\frac12},y_{k-\frac12})\right\},\quad m^{\pm}_{j,k}=\min\left\{\hat q^n_{j,k}(x_{j\pm\frac12},y_{k+\frac12}),\hat q^n_{j,k}(x_{j\mp\frac12},y_{k-\frac12})\right\},$$

and

$$\begin{aligned}
M^{+}_{j\pm\frac12,k\pm\frac12}&=\max\left\{\frac12\Big(\hat L^n_{j,k}(x_{j\pm\frac12},y_{k\pm\frac12})+\hat L^n_{j\pm1,k\pm1}(x_{j\pm\frac12},y_{k\pm\frac12})\Big),\hat q^n_{j\pm1,k\pm1}(x_{j\pm\frac12},y_{k\pm\frac12})\right\},\\
m^{+}_{j\pm\frac12,k\pm\frac12}&=\min\left\{\frac12\Big(\hat L^n_{j,k}(x_{j\pm\frac12},y_{k\pm\frac12})+\hat L^n_{j\pm1,k\pm1}(x_{j\pm\frac12},y_{k\pm\frac12})\Big),\hat q^n_{j\pm1,k\pm1}(x_{j\pm\frac12},y_{k\pm\frac12})\right\},\\
M^{-}_{j\mp\frac12,k\pm\frac12}&=\max\left\{\frac12\Big(\hat L^n_{j,k}(x_{j\mp\frac12},y_{k\pm\frac12})+\hat L^n_{j\mp1,k\pm1}(x_{j\mp\frac12},y_{k\pm\frac12})\Big),\hat q^n_{j\mp1,k\pm1}(x_{j\mp\frac12},y_{k\pm\frac12})\right\},\\
m^{-}_{j\mp\frac12,k\pm\frac12}&=\min\left\{\frac12\Big(\hat L^n_{j,k}(x_{j\mp\frac12},y_{k\pm\frac12})+\hat L^n_{j\mp1,k\pm1}(x_{j\mp\frac12},y_{k\pm\frac12})\Big),\hat q^n_{j\mp1,k\pm1}(x_{j\mp\frac12},y_{k\pm\frac12})\right\}.
\end{aligned}$$

In summary, the point values $u^{\rm N}_{j,k}$, $u^{\rm S}_{j,k}$, $u^{\rm E}_{j,k}$ and $u^{\rm W}_{j,k}$ are computed as the corresponding values of

$$\begin{aligned}
p^n_{j,k}(x,y) \;=\; &\left(\bar u^n_{j,k}-\theta^n_{j,k}\frac{(\Delta x)^2}{24}D^x_+D^x_-\bar u^n_{j,k}-\theta^n_{j,k}\frac{(\Delta y)^2}{24}D^y_+D^y_-\bar u^n_{j,k}\right)+\\
&+\Big(\theta^n_{j,k}D^x_0\bar u^n_{j,k}+(1-\theta^n_{j,k})s^x_{j,k}\Big)(x-x_j)+\Big(\theta^n_{j,k}D^y_0\bar u^n_{j,k}+(1-\theta^n_{j,k})s^y_{j,k}\Big)(y-y_k)+\\
&+\frac{\theta^n_{j,k}}{2}D^x_+D^x_-\bar u^n_{j,k}(x-x_j)^2+\theta^n_{j,k}D^x_0D^y_0\bar u^n_{j,k}(x-x_j)(y-y_k)+\frac{\theta^n_{j,k}}{2}D^y_+D^y_-\bar u^n_{j,k}(y-y_k)^2,
\end{aligned}\tag{4.17}$$

where $\theta^n_{j,k}$, $s^x_{j,k}$ and $s^y_{j,k}$ are given by (4.9) and (4.8), respectively, and the corner values $u^{\rm NE}_{j,k}$, $u^{\rm NW}_{j,k}$, $u^{\rm SE}_{j,k}$ and $u^{\rm SW}_{j,k}$ are obtained from

$$\begin{aligned}
\hat p^n_{j,k}(x,y) \;=\; &\left(\bar u^n_{j,k}-\hat\theta^n_{j,k}\frac{\Delta^2}{48}(D^{d^+}_+D^{d^+}_-+D^{d^-}_+D^{d^-}_-)\bar u^n_{j,k}\right)+\\
&+\frac{\Delta}{2\Delta x}\Big(\hat\theta^n_{j,k}(D^{d^+}_0-D^{d^-}_0)\bar u^n_{j,k}+(1-\hat\theta^n_{j,k})(\hat s^+_{j,k}-\hat s^-_{j,k})\Big)(x-x_j)+\\
&+\frac{\Delta}{2\Delta y}\Big(\hat\theta^n_{j,k}(D^{d^+}_0+D^{d^-}_0)\bar u^n_{j,k}+(1-\hat\theta^n_{j,k})(\hat s^+_{j,k}+\hat s^-_{j,k})\Big)(y-y_k)+\\
&+\hat\theta^n_{j,k}\frac{\Delta^2}{8(\Delta x)^2}\Big(D^{d^+}_+D^{d^+}_--2D^{d^+}_0D^{d^-}_0+D^{d^-}_+D^{d^-}_-\Big)\bar u^n_{j,k}(x-x_j)^2+
\end{aligned}$$

$$+\hat{\theta}^n_{j,k}\frac{\Delta^2}{4\Delta x\Delta y}\Big(D^{d^+}_+D^{d^+}_- - D^{d^-}_+D^{d^-}_-\Big)\bar{u}^n_{j,k}(x-x_j)(y-y_k)+$$
$$+\hat{\theta}^n_{j,k}\frac{\Delta^2}{8(\Delta y)^2}\Big(D^{d^+}_+D^{d^+}_- + 2D^{d^+}_0D^{d^-}_0 + D^{d^-}_+D^{d^-}_-\Big)\bar{u}^n_{j,k}(y-y_k)^2, \tag{4.18}$$

with $\hat{\theta}^n_{j,k}$, $\hat{s}^+_{j,k}$ and $\hat{s}^-_{j,k}$, given by (4.15), (4.13) and (4.14), respectively.

4.3 Two-dimensional problems

Example 4 – Two-dimensional Euler equations of gas dynamics.

We solve the two-dimensional compressible Euler equations

$$\frac{\partial}{\partial t}\begin{bmatrix}\rho\\ \rho u\\ \rho v\\ E\end{bmatrix}+\frac{\partial}{\partial x}\begin{bmatrix}\rho u\\ \rho u^2+p\\ \rho uv\\ u(E+p)\end{bmatrix}+\frac{\partial}{\partial y}\begin{bmatrix}\rho v\\ \rho uv\\ \rho v^2+p\\ v(E+p)\end{bmatrix}=0, \qquad p=(\gamma-1)\cdot\Big[E-\frac{\rho}{2}(u^2+v^2)\Big], \tag{4.19}$$

for an ideal gas, $\gamma = 1.4$, in the domain $[0,2]\times[0,0.5]\cup[0,1]\times[0.5,1]$, with the initial data corresponding to a vertical left-moving Mach 1.65 shock, positioned at $x = 1.375$. The initial shock propagates and then diffracts around a solid corner. Here ρ, u, v, p and E are the density, the x- and y-velocities, the pressure and the total energy, respectively.

We compute the solution at time $T = 0.5$, using the scheme (3.35)–(3.37), coupled with the reconstruction (4.17)–(4.18). The contour plots of the density for 128×64, 256×128, and 512×256 grid points are given in Figures 4.11, 4.12, and 4.13, respectively. The speed, $\sqrt{u^2+v^2}$, and the pressure, computed for 512×256 grid points, are shown in Figures 4.14 and 4.15.

As in [25], we obtain these results without using characteristic decomposition, dimensional splitting or evolution of nonconservative quantities. At the same time, our genuinely two-dimensional central-upwind scheme is less dissipative than the central scheme, proposed in [25], and it retains the major advantage of central schemes – *simplicity* and *efficiency*.

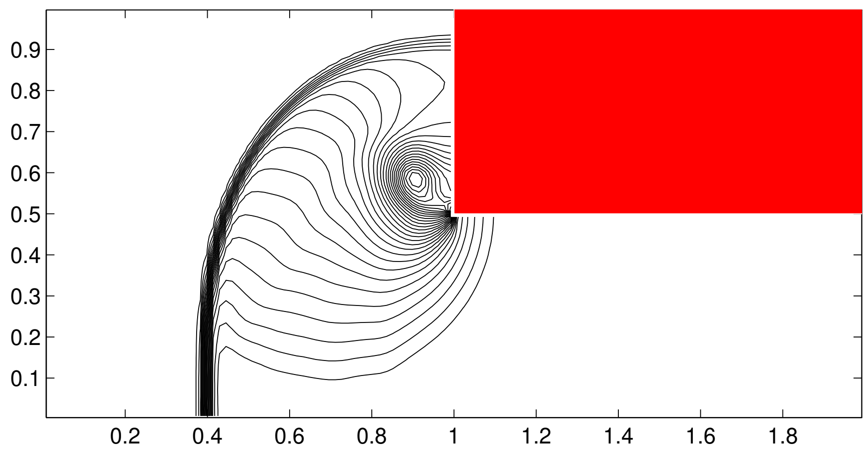

Figure 4.11: Equation (4.19), density; **T=0.5**, 128×64 grid, 30 contours.

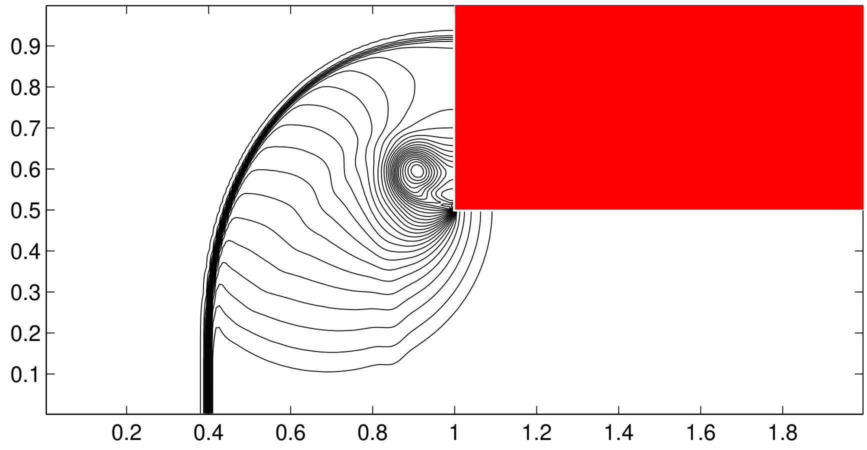

Figure 4.12: Equation (4.19), density; **T=0.5**, 256×128 grid, 30 contours.

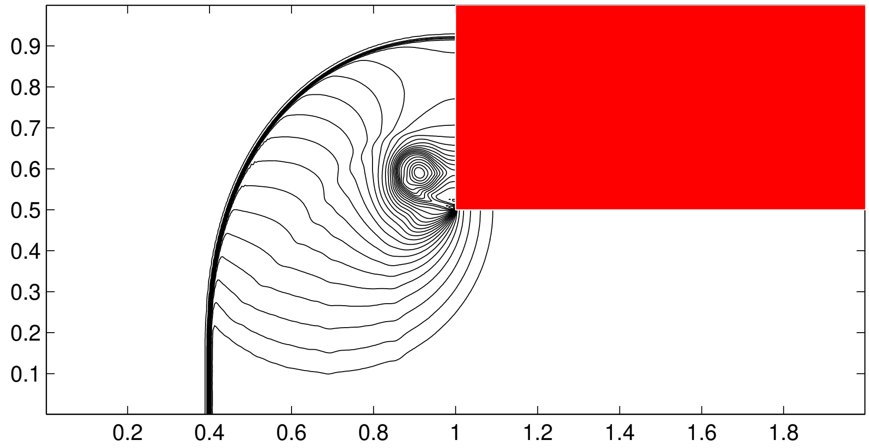

Figure 4.13: Equation (4.19), density; **T=0.5**, 512×256 grid, 30 contours.

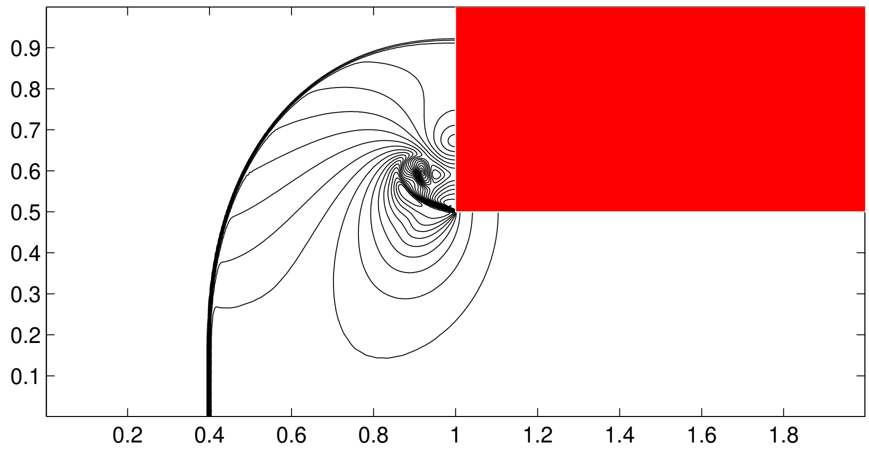

Figure 4.14: Equation (4.19), speed; **T=0.5**, 512×256 grid, 20 contours.

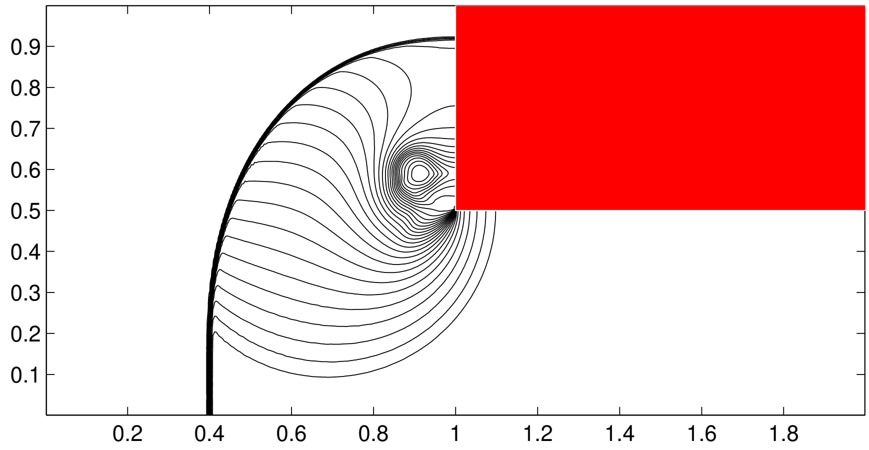

Figure 4.15: Equation (4.19), pressure; **T=0.5**, 512×256 grid, 30 contours.

Example 5 – Two-dimensional Hamilton-Jacobi equation.

In this example, we consider the two-dimensional eikonal equation of geometric optics, which is a Hamilton-Jacobi equation with a convex Hamiltonian,

$$\varphi_t + \sqrt{\varphi_x^2 + \varphi_y^2 + 1} = 0. \tag{4.20}$$

We solve equation (4.20) in the square $[0,1] \times [0,1]$, subject to the smooth periodic initial data

$$\varphi(x, y, 0) = \frac{1}{4}(\cos(2\pi x) - 1)(\cos(2\pi y) - 1) - 1. \tag{4.21}$$

The numerical solution to the Cauchy problem (4.20)–(4.21) at time $T = 0.6$ (after formation of the singularity) has been computed by the two-dimensional second-order central-upwind scheme (3.63)–(3.65). The non-oscillatory nature of the computed solution and nearly perfect resolution of the singularity can be clearly seen in Figures 4.16–4.17.

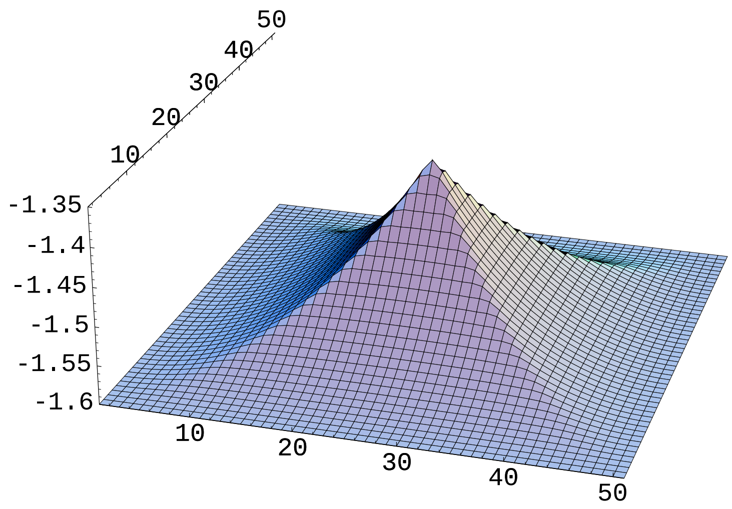

Figure 4.16: Problem (4.20)–(4.21); **T=0.6**, 50×50 grid.

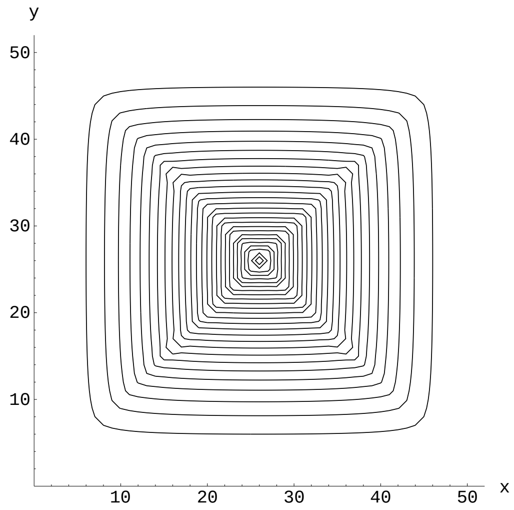

Figure 4.17: Problem (4.20)–(4.21); **T=0.6**, 50×50 grid, 30 contours.

4.4 Two-dimensional incompressible Euler and Navier-Stokes equations

Here, we consider the incompressible Euler ($\nu = 0$) and Navier-Stokes ($\nu > 0$) equations

$$\vec{u}_t + (\vec{u} \cdot \nabla)\vec{u} + \nabla p = \nu \Delta \vec{u}, \tag{4.22}$$

where p denotes the pressure and $\vec{u} = (u, v)$ is the divergence-free velocity field, satisfying $u_x + v_y = 0$. In the two-dimensional case, equation (4.22) admits an equivalent vorticity formulation, which can be written either in the conservative,

$$\omega_t + (u\omega)_x + (v\omega)_y = \nu \Delta \omega, \tag{4.23}$$

or in the transport form,

$$\omega_t + u\omega_x + v\omega_y = \nu \Delta \omega, \tag{4.24}$$

where ω is the vorticity, $\omega := v_x - u_y$. Equation (4.23) can be viewed as a two-dimensional conservation law

$$\omega_t + f(\omega)_x + g(\omega)_y = \nu \Delta \omega, \tag{4.25}$$

with a global flux $(f, g) := (u\omega, v\omega)$; while the transport equation (4.24) can be considered as a two-dimensional (viscous) Hamilton-Jacobi equation

$$\omega_t + H(\omega_x, \omega_y) = \nu \Delta \omega, \tag{4.26}$$

with a global Hamiltonian $H(\omega_x, \omega_y) = u\omega_x + v\omega_y$.

We propose two alternative Godunov-type semi-discrete central-upwind schemes for these two different formulations of the vorticity equation, (4.23) and (4.24). First, we consider (4.23) as a conservation law (4.25) and apply our two-dimensional third-order central-upwind scheme (3.35)–(3.37) to it. The resulting scheme has the conservative form

$$\frac{d}{dt}\bar{\omega}_{j,k}(t) = -\frac{H^x_{j+\frac{1}{2},k}(t) - H^x_{j-\frac{1}{2},k}(t)}{\Delta x} - \frac{H^y_{j,k+\frac{1}{2}}(t) - H^y_{j,k-\frac{1}{2}}(t)}{\Delta y} + \nu Q_{j,k}(t). \tag{4.27}$$

The following choice of the one-sided local speeds,

$$a^{\pm}_{j+\frac{1}{2},k} := \big(u_{j+\frac{1}{2},k}\big)_{\pm}, \qquad b^{\pm}_{j,k+\frac{1}{2}} := \big(v_{j,k+\frac{1}{2}}\big)_{\pm}, \tag{4.28}$$

yields the simplified numerical convection fluxes

$$\begin{aligned} H^x_{j+\frac{1}{2},k} &:= \frac{a^+_{j+\frac{1}{2},k}}{6(a^+_{j+\frac{1}{2},k}-a^-_{j+\frac{1}{2},k})}\Big[u_{j+\frac{1}{2},k+\frac{1}{2}}\omega^{\rm NE}_{j,k} + 4u_{j+\frac{1}{2},k}\omega^{\rm E}_{j,k} + u_{j+\frac{1}{2},k-\frac{1}{2}}\omega^{\rm SE}_{j,k}\Big] - \\ &- \frac{a^-_{j+\frac{1}{2},k}}{6(a^+_{j+\frac{1}{2},k}-a^-_{j+\frac{1}{2},k})}\Big[u_{j+\frac{1}{2},k+\frac{1}{2}}\omega^{\rm NW}_{j+1,k} + 4u_{j+\frac{1}{2},k}\omega^{\rm W}_{j+1,k} + u_{j+\frac{1}{2},k-\frac{1}{2}}\omega^{\rm SW}_{j+1,k}\Big], \end{aligned} \tag{4.29}$$

and

$$\begin{aligned} H^y_{j,k+\frac{1}{2}} &:= \frac{b^+_{j,k+\frac{1}{2}}}{6(b^+_{j,k+\frac{1}{2}}-b^-_{j,k+\frac{1}{2}})}\Big[v_{j-\frac{1}{2},k+\frac{1}{2}}\omega^{\rm NW}_{j,k} + 4v_{j,k+\frac{1}{2}}\omega^{\rm N}_{j,k} + v_{j+\frac{1}{2},k+\frac{1}{2}}\omega^{\rm NE}_{j,k}\Big] - \\ &- \frac{b^-_{j,k+\frac{1}{2}}}{6(b^+_{j,k+\frac{1}{2}}-b^-_{j,k+\frac{1}{2}})}\Big[v_{j-\frac{1}{2},k+\frac{1}{2}}\omega^{\rm SW}_{j,k+1} + 4v_{j,k+\frac{1}{2}}\omega^{\rm S}_{j,k+1} + v_{j+\frac{1}{2},k+\frac{1}{2}}\omega^{\rm SE}_{j,k+1}\Big]. \end{aligned} \tag{4.30}$$

The diffusion term in (4.27) is obtained by the fourth-order central differencing,

$$\begin{aligned} Q_{j,k} &= \frac{-\bar\omega_{j+2,k}+16\bar\omega_{j+1,k}-30\bar\omega_{j,k}+16\bar\omega_{j-1,k}-\bar\omega_{j-2,k}}{12(\Delta x)^2} + \\ &+ \frac{-\bar\omega_{j,k+2}+16\bar\omega_{j,k+1}-30\bar\omega_{j,k}+16\bar\omega_{j,k-1}-\bar\omega_{j,k-2}}{12(\Delta y)^2}. \end{aligned} \tag{4.31}$$

The intermediate values of the velocities, required to compute the convection fluxes (4.29) and (4.30), are approximated by the fourth-order averaging, namely

$$u_{j+\frac{1}{2},k} = \frac{-u_{j+2,k}+9u_{j+1,k}+9u_{j,k}-u_{j-1,k}}{16}, \qquad v_{j,k+\frac{1}{2}} = \frac{-v_{j,k+2}+9v_{j,k+1}+9v_{j,k}-v_{j,k-1}}{16}. \tag{4.32}$$

The velocities at the grid points, $\{u_{j,k}, v_{j,k}\}$, are recovered from the computed vorticities $\{\omega_{j,k}\}$ at every time step. This is done with the help of the stream-function ψ, such that $u = \psi_y$, $v = -\psi_x$, and $\Delta\psi = -\omega$. We solve this Poisson equation by the nine-point Laplacian approximation. Then, having the values of $\{\psi_{j,k}\}$, we compute the velocities

$$u_{j,k} = \frac{-\psi_{j,k+2}+8\psi_{j,k+1}-8\psi_{j,k-1}+\psi_{j,k-2}}{12\Delta y}, \qquad v_{j,k} = \frac{\psi_{j+2,k}-8\psi_{j+1,k}+8\psi_{j-1,k}-\psi_{j-2,k}}{12\Delta x}. \tag{4.33}$$

This completes the construction of the 'conservative' central-upwind scheme for the incompressible Euler and Navier-Stokes equations.

We now apply this scheme, coupled with the reconstruction (4.17)–(4.18), to the Navier-Stokes equation (4.23) with $\nu = 0.05$, augmented with the smooth periodic initial data

$$u(x,y,0) = -\cos x \sin y, \qquad v(x,y,0) = \sin x \cos y, \tag{4.34}$$

This test-problem, proposed in [9], admits the exact classical solution, given by

$$u(x,y,t) = -e^{-2\nu t}\cos x \sin y, \qquad v(x,y,t) = e^{-2\nu t}\sin x \cos y.$$

$Nx \times Ny$	L^∞-error	rate	L^1-error	rate	L^2-error	rate
32×32	2.103e-03	–	2.761e-02	–	5.623e-03	–
64×64	2.788e-04	2.92	3.652e-03	2.92	7.404e-04	2.92
128×128	3.548e-05	2.97	4.636e-04	2.98	9.385e-05	2.98
256×256	4.444e-06	3.00	5.811e-05	3.00	1.176e-05	3.00

Table 4.2: Accuracy test for the third-order 'conservative' scheme for the Navier-Stokes equation (4.23),(4.34), $\nu = 0.05$; errors at **T=2**.

In this numerical experiment, we check the accuracy of our scheme. The numerical solution is computed at time $T = 2$, and the errors for the vorticity, measured in the L^∞-, L^1- and L^2-norms, are presented in Table 4.2. These results indicate the expected third-order accuracy of the proposed scheme (4.27)–(4.33).

Next, we apply the scheme (4.27)–(4.33) together with the reconstruction (4.17)–(4.18) to the Euler equation, (4.23) with $\nu = 0$, subject to the $(2\pi, 2\pi)$-periodic initial data

$$u(x,y,0) = \begin{cases} \tanh(\frac{1}{\rho}(y - \pi/2)), & y \le \pi, \\ \tanh(\frac{1}{\rho}(3\pi/2 - y)), & y > \pi, \end{cases} \qquad v(x,y,0) = \delta \cdot \sin x. \tag{4.35}$$

This is the double shear-layer model problem, proposed in [7]. We take $\rho = \pi/15$ and $\delta = 0.05$. Figures 4.18 and 4.20 are the contour plots (30 contours) of the solution at time $T = 10$ with 64×64 and 128×128 grid points, respectively. The three-dimensional plots of the same results are shown in Figures 4.19 and 4.21. The performed numerical experiments demonstrate that our scheme provides a very high resolution. These results are comparable with the results obtained by the third-order semi-discrete central scheme in [25].

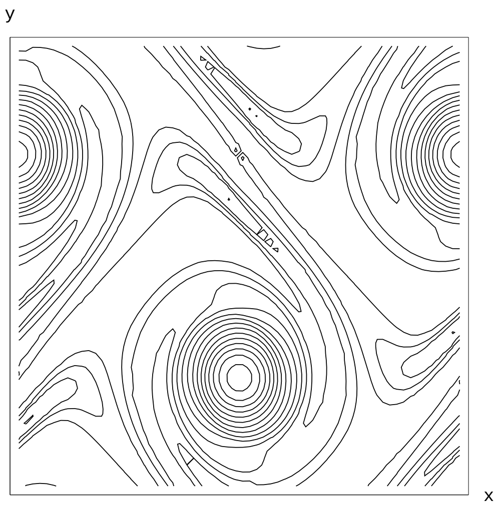

Figure 4.18: Solution of the incompressible Euler equation, computed by the 'conservative' scheme; 64×64 grid.

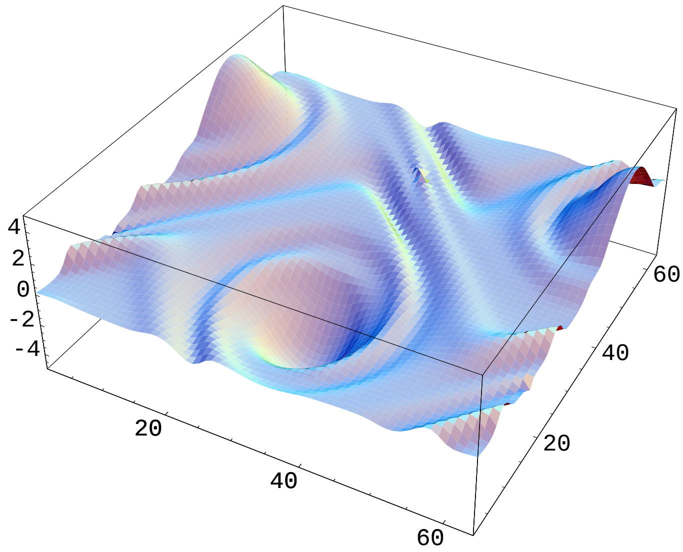

Figure 4.19: Solution of the incompressible Euler equation, computed by the 'conservative' scheme; 64×64 grid.

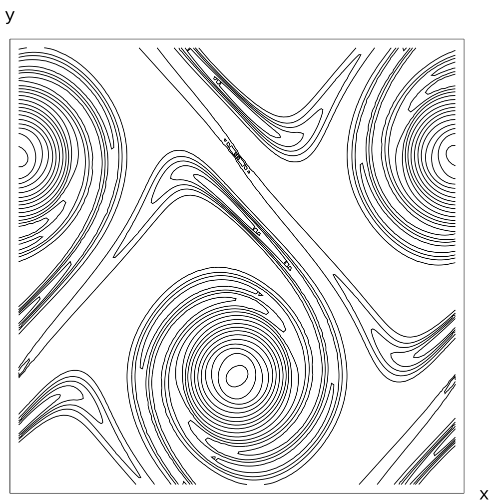

Figure 4.20: Solution of the incompressible Euler equation, computed by the 'conservative' scheme; 128×128 grid.

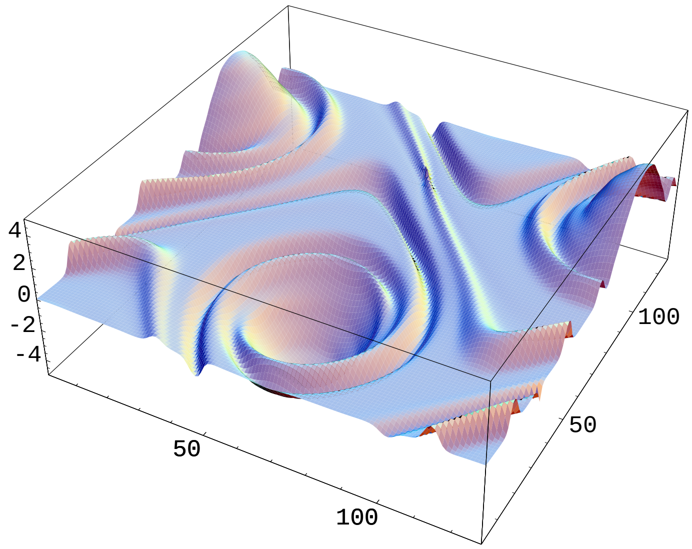

Figure 4.21: Solution of the incompressible Euler equation, computed by the 'conservative' scheme; 128×128 grid.

The second alternative is to solve the vorticity equation in its transport form, (4.24), which can be viewed as a Hamilton-Jacobi equation (4.26).

We choose the one-sided local speeds to be

$$a^{\pm}_{j,k} := (u_{j,k})_{\pm}, \qquad b^{\pm}_{j,k} := (v_{j,k})_{\pm}, \tag{4.36}$$

and in this setting, our two-dimensional second-order central-upwind scheme (3.63)–(3.65) has the following simple form

$$\begin{aligned}\frac{d}{dt}\varphi_{j,k}(t) \;=\; & -\frac{a^-_{j,k}b^-_{j,k}(u_{j,k}\omega^+_x+v_{j,k}\omega^+_y)-a^-_{j,k}b^+_{j,k}(u_{j,k}\omega^+_x+v_{j,k}\omega^-_y)}{(a^+_{j,k}-a^-_{j,k})(b^+_{j,k}-b^-_{j,k})}+\\ & +\frac{a^+_{j,k}b^-_{j,k}(u_{j,k}\omega^-_x+v_{j,k}\omega^+_y)-a^+_{j,k}b^+_{j,k}(u_{j,k}\omega^-_x+v_{j,k}\omega^-_y)}{(a^+_{j,k}-a^-_{j,k})(b^+_{j,k}-b^-_{j,k})}+\nu L_{j,k}.\end{aligned} \tag{4.37}$$

Here, $w^{\pm}_x$, $w^{\pm}_y$ are given by (3.64), and the term $L_{j,k}$ stands for the standard central difference approximation of the linear viscous term, that is

$$L_{j,k}=\frac{\omega_{j+1,k}-2\omega_{j,k}+\omega_{j-1,k}}{(\Delta x)^2}+\frac{\omega_{j,k+1}-2\omega_{j,k}+\omega_{j,k-1}}{(\Delta y)^2}. \tag{4.38}$$

As in the 'conservative' scheme, we recover the velocities $\{u_{j,k}, v_{j,k}\}$ from the known values of the vorticity $\{\omega_{j,k}\}$, using the stream-function approach. At each time step we solve the five-points Laplacian $\Delta\psi_{j,k}=-\omega_{j,k}$, and compute the velocities as follows,

$$u_{j,k}=\frac{\psi_{j,k+1}-\psi_{j,k-1}}{2\Delta y}, \qquad v_{j,k}=-\frac{\psi_{j+1,k}-\psi_{j-1,k}}{2\Delta x}. \tag{4.39}$$

We now apply this second-order 'transport' scheme to the initial boundary value problem for the Navier-Stokes equation (4.24),(4.34) with $\nu=0.05$. The numerical solution of this test problem is computed at time $T=2$, and the L^∞-, L^1- and L^2-errors for the vorticity are presented in Table 4.3. These results indicate the second-order convergence rate measured in all these norms. We would also like to point out that the absolute values of the errors here are about 10 times smaller, than the corresponding errors obtained by the semi-discrete central scheme in [27, Table 6.1].

$Nx\times Ny$	L^∞-error	rate	L^1-error	rate	L^2-error	rate
32×32	5.559e-03	–	7.304e-02	–	1.492e-02	–
64×64	1.672e-03	1.73	2.265e-02	1.69	4.574e-03	1.71
128×128	4.531e-04	1.88	6.263e-03	1.85	1.250e-03	1.87
256×256	1.176e-04	1.95	1.644e-03	1.93	3.276e-04	1.93

Table 4.3: Accuracy test for the second-order 'transport' scheme for the Navier-Stokes equation (4.24),(4.34), $\nu=0.05$; errors at **T=2**.

Finally, we test our scheme (4.36)–(4.39) on the double shear-layer problem (4.24),(4.35). The contour plots (30 contours) of the solution are shown in Figures 4.22, 4.24 and 4.26, where the computations are performed at time $T=10$ with 64×64, 128×128, and 256×256 grid points. The corresponding three-dimensional plots are presented in Figures 4.23, 4.25 and 4.27.

We would like to point out that our second-order 'transport' scheme (4.36)–(4.39) has a very high resolution. The numerical experiments show that it is far superior to the second-order semi-discrete central scheme in [27, Figures 6.7–6.10]. This improvement is attributed to the smaller numerical viscosity present in the central-upwind scheme. Moreover, the resolution of (4.36)–(4.39) is almost as good as the resolution of our third-order 'conservative' scheme (Figures 4.18–4.21).

As in [27, Figures 6.9–6.10], our numerical solution has spurious spikes, but of smaller heights. Also, the consequitive mesh refinements (Figures 4.22–4.27) clearly demonstrate, that the supports of these spikes diminish as the mesh size decreases.

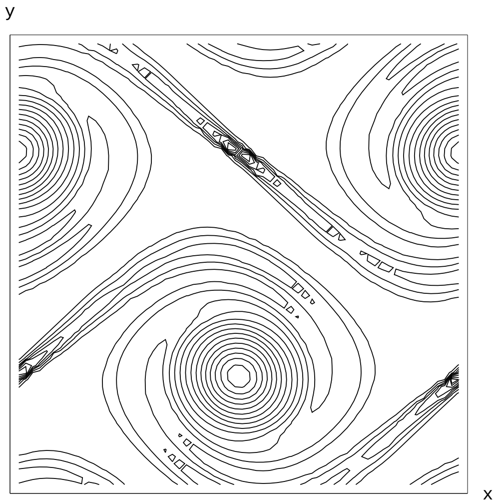

Figure 4.22: Solution of the incompressible Euler equation, computed by the 'transport' scheme; 64 × 64 grid.

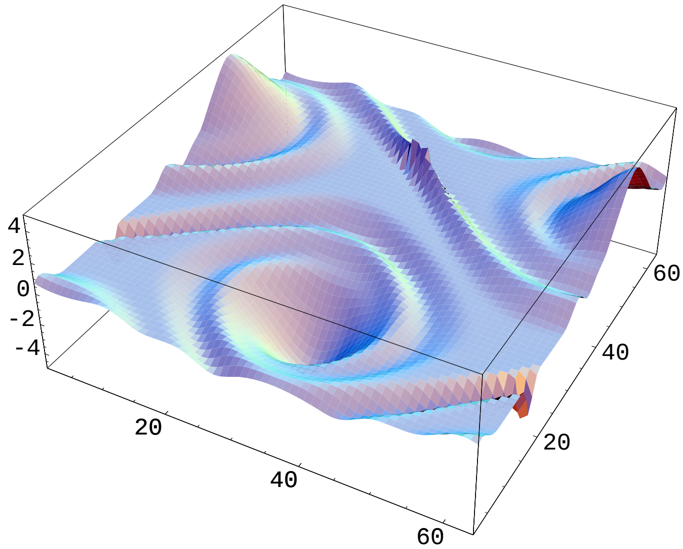

Figure 4.23: Solution of the incompressible Euler equation, computed by the 'transport' scheme; 64 × 64 grid.

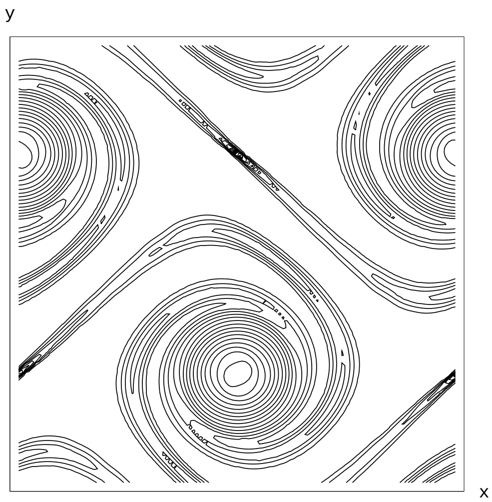

Figure 4.24: Solution of the incompressible Euler equation, computed by the 'transport' scheme; 128 × 128 grid.

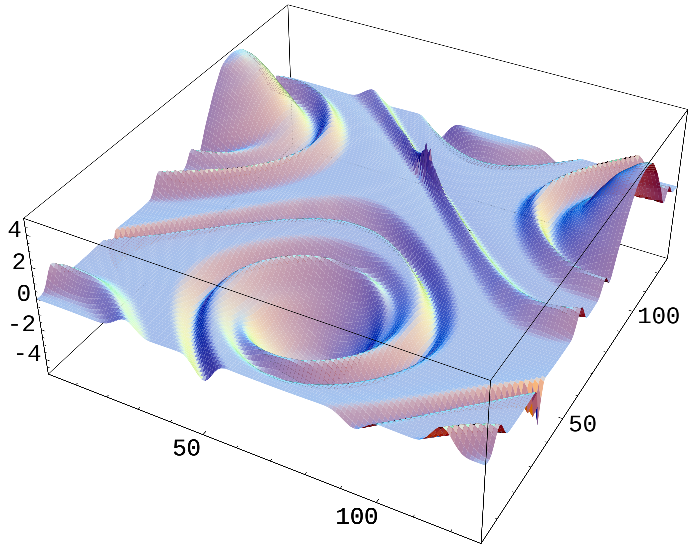

Figure 4.25: Solution of the incompressible Euler equation, computed by the 'transport' scheme; 128 × 128 grid.

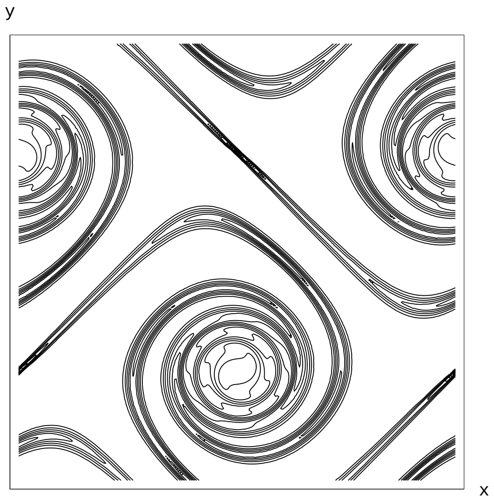

Figure 4.26: Solution of the incompressible Euler equation, computed by the 'transport' scheme; 256×256 grid.

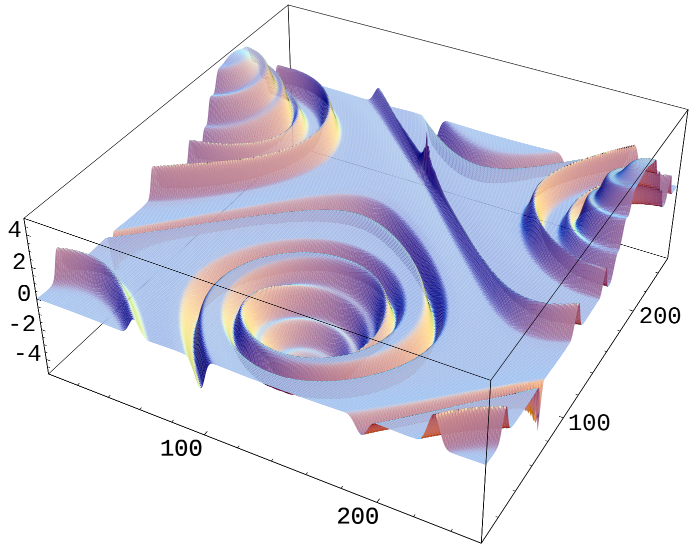

Figure 4.27: Solution of the incompressible Euler equation, computed by the 'transport' scheme; 256×256 grid.

Acknowledgment: The work of A. Kurganov was supported in part by the NSF Group Infrastructure Grant. Part of the work of S. Noelle, as well as a visit of A. Kurganov at Bonn University, were sponsored by DFG Grant SFB256.

References

[1] R. Abgrall, *Numerical discretization of first-order Hamilton-Jacobi equation on triangular meshes*, Comm. Pure Appl. Math., 49 (1996), pp. 1339–1373.

[2] A. M. Anile, V. Romano and G. Russo, *Extended hydrodynamical model of carrier transport in semiconductors*, SIAM J. Appl. Math., Preprint.

[3] P. Arminjon and M.-C. Viallon, *Généralisation du schéma de Nessyahu-Tadmor pour une équation hyperbolique à deux dimensions d'espace*, C.R. Acad. Sci. Paris, t. 320, série I (1995), pp. 85–88.

[4] P. Arminjon, D. Stanescu and M.-C. Viallon, *A two-dimensional finite volume extension of the Lax-Friedrichs and Nessyahu-Tadmor schemes for compressible flows*, Proc. 6th. Int. Symp. on CFD, Lake Tahoe, M. Hafez and K. Oshima (eds.), Vol. IV (1995), pp. 7–14.

[5] P. Arminjon, M.-C. Viallon and A. Madrane, *A finite volume extension of the Lax-Friedrichs and Nessyahu-Tadmor schemes for conservation laws on unstructured grids*, Int. J. Comp. Fluid Dyn., 9 (1997), pp. 1–22.

[6] P. Arminjon and M.-C. Viallon, *Convergence of a finite volume extension of the Nessyahu-Tadmor scheme on unstructured grids for a two-dimensional linear hyperbolic equation*, SIAM J. Numer. Anal., 36 (1999), pp. 738–771.

[7] J.B. BELL, P. COLELLA, H.M. GLAZ, *A second-order projection method for the incompressible Navier-Stokes equations*, J. of Comp. Phys., 85 (1989), pp. 257–283.

[8] F. BIANCO, G. PUPPO AND G. RUSSO, *High order central schemes for hyperbolic systems of conservation laws*, SIAM J. Sci. Comp., to appear.

[9] A. CHORIN, *Numerical solution of the Navier-Stokes equations*, Math. Comp., 22 (1968), pp. 745–762.

[10] L. CORRIAS, M. FALCONE AND R. NATALINI, *Numerical schemes for conservation laws via Hamilton-Jacobi equations*, Math. Comp., 64 (1995), pp. 555–580.

[11] M. G. CRANDALL AND P.-L. LIONS, *Two approximations of solutions of Hamilton-Jacobi equations*, Math. Comp., 43 (1984), pp. 1–19.

[12] B. EINFELD, *On Godunov-type methods for gas dynamics* SIAM J. Numer. Anal., 25 (1988), pp. 294–318.

[13] B. ENGQUIST AND O. RUNBORG, *Multi-phase computations in geometrical optics*, J. Comp. Appl. Math., 74 (1996), pp. 175–192.

[14] K.O. FRIEDRICHS, *Symmetric hyperbolic linear differential equations*, Comm. Pure Appl. Math., 7 (1954), pp. 345–392.

[15] A. HARTEN, *High resolution schemes for hyperbolic conservation laws*, J. of Comp. Phys., 49 (1983), pp. 357–393.

[16] A. HARTEN, B. ENGQUIST, S. OSHER AND S.R. CHAKRAVARTHY, *Uniformly high order accurate essentially non-oscillatory schemes III*, J. of Comp. Phys., 71 (1987), pp. 231–303.

[17] A. HARTEN, P. LAX AND B. VAN LEER, *On upstream differencing and Godunov-type schemes for hyperbolic conservation laws*, SIAM Rev., 25, no. 1 (1983), pp. 35–61.

[18] G.-S. JIANG AND C.-W. SHU, *Efficient implementation of weighted ENO schemes*, J. of Comp. Phys., 126 (1996), pp. 202–228.

[19] G.-S. JIANG AND E. TADMOR, *Non-oscillatory central schemes for multidimensional hyperbolic conservation laws*, SIAM J. Sci. Comp., 19 (1998), pp. 1892–1917.

[20] R. KUPFERMAN, *Simulation of viscoelastic fluids; Couette-Taylor flow*, J. of Comp. Phys., to appear.

[21] R. KUPFERMAN, *A numerical study of the axisymmetric Couette-Taylor problem using a fast high-resolution second-order central scheme*, SIAM J. Sci. Comp., 20 (1998), pp. 858–877.

[22] R. KUPFERMAN AND E. TADMOR, *A fast high-resolution second-order central scheme for incompressible flows*, Proceedings of the National Academy of Sciences, 94 (1997), pp. 4848–4852.

[23] A. KURGANOV, *Conservation laws: stability of numerical approximations and nonlinear regularization*, Ph.D. Thesis, Tel-Aviv University, Israel (1997).

[24] A. KURGANOV AND D. LEVY, *A third-order semi-discrete central scheme for conservation laws and convection-diffusion equations*, submitted to SIAM J. Sci. Comp.

[25] A. KURGANOV, S. NOELLE AND G. PETROVA, *A third-order semi-discrete genuinely multidimensional central scheme for hyperbolic conservation laws and related problems*, submitted to Numerische Mathematik.

[26] A. KURGANOV AND E. TADMOR, *New high-resolution central schemes for nonlinear conservation laws and convection-diffusion equations*, submitted to J. of Comp. Phys.

[27] A. KURGANOV AND E. TADMOR, *New high-resolution semi-discrete schemes for Hamilton-Jacobi equations*, submitted to J. of Comp. Phys.

[28] P.D. LAX, *Weak solutions of nonlinear hyperbolic equations and their numerical computation*, Comm. Pure Appl. Math., 7 (1954), pp. 159–193.

[29] B. VAN LEER, *Towards the ultimate conservative difference scheme, V. A second order sequel to Godunov's method*, J. of Comp. Phys., 32 (1979), pp. 101–136.

[30] D. LEVY, G. PUPPO AND G. RUSSO, *Central WENO schemes for hyperbolic systems of conservation laws*, Math. Model. and Numer. Anal., 33, no. 3 (1999), pp. 547–571.

[31] D. LEVY, G. PUPPO AND G. RUSSO, *A third order central WENO scheme for 2D conservation laws*, Appl. Numer. Math., to appear.

[32] D. LEVY, G. PUPPO AND G. RUSSO, *Compact central WENO schemes for multidimensional conservation laws*, submitted.

[33] D. LEVY AND E. TADMOR, *Non-oscillatory central schemes for the incompressible 2-D Euler equations*, Math. Res. Lett., 4 (1997), pp. 1–20.

[34] K.-A. LIE AND S.NOELLE, *Remarks on high-resolution non-oscillatory central schemes for multidimensional systems of conservation laws. Part I: An improved quadrature rule for the flux-computation.* Submitted to SIAM J. Sci. Comp.. *Part II: Artificial compression* (to be submitted). *Part III: Stability* (to be submitted).

[35] C.-T. LIN AND E. TADMOR, *L^1-stability and error estimates for approximate Hamilton-Jacobi solutions*, Numerische Mathematik.

[36] C.-T. LIN AND E. TADMOR, *High-resolution non-oscillatory central schemes for Hamilton-Jacobi Equations*, SIAM J. Sci. Comp., to appear.

[37] X.-D. LIU AND S. OSHER, *Nonoscillatory high order accurate self similar maximum principle satisfying shock capturing schemes. I*, SIAM J. Numer. Anal., 33 (1996), pp. 760–779.

[38] X.-D. LIU, S. OSHER AND T. CHAN, *Weighted essentially non-oscillatory schemes*, J. of Comp. Phys., 115 (1994), pp. 200–212.

[39] X.-D. LIU AND E. TADMOR, *Third order nonoscillatory central scheme for hyperbolic conservation laws*, Numerische Mathematik, 79 (1998), pp. 397–425.

[40] H. NESSYAHU AND E. TADMOR, *Non-oscillatory central differencing for hyperbolic conservation laws*, J. Comp. Phys., 87 (1990), pp. 408–463.

[41] S. NOELLE, *A comparison of third and second order accurate finite volume schemes for the two-dimensional compressible Euler equations*, Proceedings of the Seventh International Conference on Hyperbolic Problems, Zürich 1998. Intern. Ser. Numer. Math. 129, 757–766 (Birkhäuser).

[42] S. Osher and C.-W. Shu, *High-order essential nonoscillatory schemes for Hamilton-Jacobi equations*, SIAM J. Numer. Anal., 28 (1991), pp. 907–922.

[43] S. Osher and E. Tadmor, *On the convergence of difference approximations to scalar conservation laws*, Math. Comp., 50 (1988), pp. 19–51.

[44] V. Romano and G. Russo, *Numerical solution for hydrodynamical models of semiconductors*, M^3AN, Preprint.

[45] C.-W. Shu, *Total-variation-diminishing time discretizations*, SIAM J. Sci. Comp., 6 (1988), pp. 1073–1084.

[46] C.-W. Shu, *Numerical experiments on the accuracy of ENO and modified ENO schemes*, J. Sci. Comp., 5, vol. 2 (1990), pp. 127–149.

[47] C.-W. Shu and S. Osher, *Efficient implementation of essentially non-oscillatory shock-capturing schemes*, J. Comp. Phys., 77 (1988), pp. 439–471.

[48] P.E. Souganidis, *Approximation schemes for viscosity solutions of Hamilton-Jacobi equations*, J. Diff. Eqs., 59 (1985), pp. 1–43.

[49] Y.C. Tai, S. Noelle, N. Gray and K. Hutter, *Shock capturing and front tracking methods for granular avalanches*, preprint, to be submitted to J. Comp. Phys.

[50] B. Wendroff, *Approximate Riemann solvers, Godunov schemes, and contact discontinuities*, to appear in *Godunov methods: theory and applications*, E. F. Toro (editor), Kluwer Academic/Plenum Publishers (2000).

[51] P. Woodward and P. Colella, *The numerical solution of two-dimensional fluid flow with strong shocks*, J. Comp. Phys., 54 (1988), pp. 115–173.